Fabrication of a Biodegradable Piezoelectric-Based Wearable Sensor for Non-invasive Monitoring of Dynamic Human Motions and Physiological Signals

by

Mohsin Ali

A Dissertation Submitted to the
Graduate School of Sciences and Engineering
in Partial Fulfillment of the Requirements for
the Degree of

Master of Science

in

Biomedical Science and Engineering

KOÇ
ÜNİVERSİTESİ

Fabrication of a Biodegradable Piezoelectric-Based Wearable Sensor for Non-invasive Monitoring of Dynamic Human Motions and Physiological Signals

August, 2023

Koç University

Graduate School of Sciences and Engineering

This is to certify that I have examined this copy of a master's thesis by

Mohsin Ali

and have found that it is complete and satisfactory in all respects,

and that any and all revisions required by the final

examining committee have been made.

Committee Members:

Asst. Prof. Dr. Levent Beker (Advisor)

Asst. Prof. Emin Istif

Prof. Ipek Basdogan

Date: _____

To my beloved parents, siblings, and friends!

ABSTRACT

Fabrication of a Biodegradable Piezoelectric-Based Wearable Sensor for Non-invasive Monitoring of Dynamic Human Motions and Physiological Signals

Master of Science in Biomedical Science and Engineering

August, 2023

Recent advancements in flexible sensors and piezoelectric materials have facilitated the progress of continuous monitoring systems in the form of wearable and implantable medical devices, enabling the monitoring of human physiological signals. However, the non-degradable nature of these materials has resulted in the accumulation of significant amounts of electronic waste (e-waste) and necessitated subsequent surgeries for device removal. In this study, we introduce a flexible and biodegradable piezoelectric material fabricated specifically for wearable and implantable devices. This material addresses the issues associated with secondary surgeries and e-waste, while providing a high-performance platform for the continuous and seamless monitoring of human physiological signals and tactile stimuli. The innovative combination of bioresorbable poly (L-lactic acid) (PLLA) and glycine has resulted in the development of flexible piezoelectric devices capable of non-invasive measurement of artery pulse signals in near-surface arteries and detecting slight muscle movements, including those of the trachea, esophagus, and joints. Furthermore, we demonstrate the complete degradability of the piezoelectric film in a phosphate buffer saline (PBS) solution at a temperature of 37°C. The pressure sensor derived from this material exhibits a high sensitivity of 13.2 mV/kPa, with a response time of 10 ms, and demonstrates excellent mechanical stability. Additionally, this piezoelectric material showcases comparable performance to commonly used non-degradable counterparts for measuring physiological signals. Due to its degradable nature, it can also be employed in temporary implantable medical devices for monitoring purposes.

Keywords: Biodegradable devices, Biodegradable piezoelectric polymer, Health monitoring, Radial artery, Carotid artery

ÖZETÇE

Dinamik insan hareketlerinin ve fizyolojik sinyallerin non-invaziv izlenmesi için biyobozunur piezoelektrik tabanlı giyilebilir sensör üretimi

Biyomedikal Bilimler ve Mühendislik Bilim Ustası

Ağustos, 2023

Son zamanlardaki esnek sensörler ve piezoelektrik malzemelerdeki ilerlemeler, sürekli takip sistemlerinin, giyilebilir ve implant edilebilir tıbbi cihazlar şeklinde geliştirilmesini sağlamıştır. Bununla birlikte, bunların parçalanamayan özellikleri aynı zamanda önemli miktarda parçalanamayan elektronik atık (e-atık) oluşumuna ve implant çıkarılması için ikincil bir cerrahi işleme ihtiyaç duyulmasına yol açmıştır. Burada, ikincil cerrahi ve e-atık sorununu çözen, aynı zamanda insan fizyolojik sinyallerin ve dokunsal uyarıların sürekli ve kesintisiz izlenmesi için yüksek performanslı bir platform sunan giyilebilir ve implant edilebilir cihazlar için esnek ve biyolojik olarak parçalanabilen bir piezoelektrik malzeme sunmaktayız. Yeni bir PLLA ve glisin biyolojik olarak parçalanabilen bileşimi, yüzey yakını arterlerde nabız sinyallerinin ve kasların hafif hareketlerinin (trakea, özofagus ve eklem hareketleri dahil) invaziv olmayan ölçümü için esnek piezoelektrik cihazlar geliştirmiştir. Ayrıca, 37 oC'de PBS içinde piezoelektrik filmin tamamen parçalanabilirliğini göstermekteyiz. Geliştirilen basınç sensörü, 10 ms yanıt süresiyle 13,2 mV/kPa yüksek hassasiyete sahiptir ve iyi mekanik stabilite sergilemektedir. Bu piezoelektrik malzeme, fizyolojik sinyallerin ölçülmesi için yaygın olarak kullanılan parçalanamayan piezoelektrik malzemelerle karşılaştırılabilir performansa sahiptir. Ayrıca, parçalanabilme özelliği nedeniyle geçici implant edilebilir tıbbi cihazlarda da izleme için kullanılabilir.

Anahtar kelimeler: Biyolojik olarak parçalanabilir cihazlar, Biyolojik olarak parçalanabilen piezoelektrik polimer, Sağlık izleme, Radyal arter, Karotid arter

AKNOWLEDGEMENTS

First of all, I would like to express my deepest gratitude to my supervisor Dr. Levent Beker for providing with me an opportunity to work in Bio-Integrated Microdevices Laboratory (BMDL), for his guidance and support along with my Masters. I would also like to thank Dr. Emin Istif for the invaluable scientific advice and relevant comments. Your passion in science always drives me back on the right track.

I am also grateful to Prof. Ipek Basdogan for accepting to be jury members for reviewing my thesis work as well as for allowing us to use dynamic mechanical shaker from her lab.

It is my pleasure to work in a group having a great atmosphere in the office and the lab with inspiring colleagues. I would like to thank the current members, Taher Abbasi, Ritu Das, Muhammad Awais, Fariborz Mirlou, Alp, Umut, Rumeysa, Pelin, Buse, Miray, Emine and Deniz for making my MS journey enjoyable with memorable work and after-work times.

I would like to warmly thank all the staff members from the N2star cleanroom and KUYTAM for their expertise and services. Without the great facilities you have provided and maintained day after day, I would not have been able to complete my thesis.

Throughout my master's life, I had the pleasure to connect deeply with the Pakistani community here at Koç University. Without these delighting and cheering moments, we had, my life in Turkey would have become less enjoyable.

Last but not least, I would like to thank my family for allowing and supporting me to do whatever things I would like to do. I would also like to express my deepest gratitude to my Parents and siblings. I would not have finished this journey without your heart-warming and endless support. Finally, I would like to express my thanks to my friends; Hisham Butt, Muhammad Umer Abid, and Muhammad Ahmad for their encouragement and support.

TABLE OF CONTENTS

List of Figures ix

List of tables xi

Abbreviations xii

Chapter 1: Introduction 1

1.1 This work 6

1.2 Thesis outline 7

Chapter 2: Literature review 8

2.1 Natural Biodegradable Piezoelectric Polymers 9

2.1.1 Proteins and their derivatives 9

2.1.2 Polysaccharide 14

2.1.3 Animal-derived piezoelectrics 16

2.1.4 Virus 18

2.2 Synthetic Biodegradable Piezoelectric Polymers 20

Chapter 3: Materials and methods 25

3.1 Flexible piezoelectric PLLA/Gly film preparation: 26

3.2 Fabrication of PLLA/Gly thin film wearable Sensor: 26

3.3 Vibration system for piezoelectricity measurement: 27

3.4 Impact system for piezoelectricity measurement: 27

3.5 Amplification: 28

3.6 The dielectric constant calculation: 28

3.7 Herman's Orientation Function: 28

3.8 Characterization of PLLA/Gly film: 29

3.9 Differential scanning calorimetry: 29

3.10 Fourier transform infrared spectroscopy: 30

3.11 Current and power density measurmen: 30
Chapter 4: Results and discussion 31
4.1 Fabrication of wearable piezoelectric sensor 32
4.2 Structural and morphological analysis 34
4.3 Piezoelectric characterization 41
4.3.1 D_{33} coefficient measurement 47
4.4 Real-time monitoring of human physiological signals 47
4.5 Current and power density measurement 51
4.6 51
4.7 Biodegradation of PLLA/Gly-10 film 52
Chapter 5: Coclusion 53
Bibliography 56

LIST OF FIGURES

Figure 1.1: Applications of common piezoelectric materials.. 3

Figure 2.1: Protein and its derivatives-based devices..... 14

Figure 2-2: Polysacharide based devices 20

Figure 2-3: Synthetic polymer based piezoelectric devices 24

Figure 3.2: Optical image of vibration testing setup 27

Figure 3.3: Optical photograph of impact testing setup 28

Figure 4-1: a) Schematic demonstration of the fabrication process for biodegradable piezoelectric PLLA/Gly film and wearable healthmonitoring sensor……34

Figure 4.2: Characterization of crystallinity and polymer chain orientation for PLLA/Gly films. a) One-dimensional (1D) XRD results for PLLA/Gly films with different weight% of glycine. b) Two-dimensional XRD photographs depict the orientation of the polymer chain of PLLA films with different glycine content..... 36

Figure 4-3: Percent degree of crystallinity of PLLA/Gly films as a function of glycine content. 37

Figure 4-4**:** DSC thermograms of neat PLLA and PLLA/Gly films 37

Figure 4-5**:** (a-b) FTIR spectra of neat PLLA and PLLA/Gly films in the range of 800-4000 cm^{-1}. (c) Schematic illustration of intermolecular hydrogen between PLLA and glycine molecules. 39

Figure 4-6**:** a-c) SEM images of crystallized PLLA/Gly-10 film at ambient conditions. d) Schematic illustration of crystalline structure comprises crystal lamellae connected by amorphous regions. 40

Figure 4-7**:** Measurmenet of piezoelectriciy under vibraiton and impact testing.... 42

Figure 4-8**:** Voltage output generated by piezoelectric pressure sensor under different dynamic impact loading (force). 43

Figure 4-9**:** a) A typical calibration curve generated from PLLA/Gly-10 sensor under different input pressures. The piezoelectric sensor displays good linearity and sensitivity ranging from 3.2 to 69.5 kPa. b) Response time of PLLA/Gly-10. c) Output signals from commercial (PCB piezotronics sensor) and PLLA/Gly-10 sensor. d) Long-term (mechanical) durability test of the piezoelectric sensor under dynamic loading conditions with impact pressure of (31.25 kPa) and frequency of 5 Hz. The inset demonstrates an enlarged view of voltage output versus time. 45

Figure 4-10**:** Non-invasive physiological signal monitoring. 50

Figure 4-11**:** a) Change in current, output voltage and (b) instantaneous output power density as a funciton of load resistances ranging from 100 kΩ- 10 MΩ. 51

Figure 4-12**:** Degradation of PLLA/Gly film in PBS solution. 52

LIST OF TABLES

Table 3-1: Sample information 26
Table 4-1: Comparison of performance of different mechanical sensors 46

ABBREVIATIONS

PZT	Lead Zirconium Titanate
$BaTiO_3$	Barium Titanate
KNN	Potassium Sodium Niobate
$LiNbO_3$	Lithium Niobate
BNT	Bismuth Sodium Titanate
IMDs	Implantable Medical Devices
PVDF-TrFE	Polyvinylidene Fluoride-Triflouroethylene
HF	Heart failure
PLLA	Poly (L-Lactic Acid)
HMI	Human Machine Interface
ZnO	Zinc Oxide
Gly	Glycine
PBS	Phosphate Buffer Saline
CS	Chitosan
DFT	Density Functional Theory
AlN	Aluminium Nitride
FF	Diphenylalanine
PFM	Piezo Force Microscopy
PNT	Peptide Nanotube
PENG	Piezoelectric Nano Generator
THPP	Tetra Hydroxyphenyl Porphyrin
CNC	Cellulose Nano Crystals
CNF	Cellulose Nano Fibers
OS	Onion Skin
SF	Silk Fibroins
SS	Spider Silk
AAO	Aluminium Oxide Template
PLA	Poly (Lactic Acid)
XRD	X-Ray Diffraction
PHBV	Pol(3-Hydroxybutyrate-Co-3-Hydroxyvalerate)

PDLA	Poly(D-Lactic Acid)
PMs	Particulate Matters
PVA	Polyvinyl Alcohol
HOF	Herman's Orientation Function
WAXS	Wide Angle X-ray Scattering
SEM	Scanning Electron Microscopy
DSC	Differential Scanning Calorimetry
FTIR	Fourier Transform Infrared Spectroscopy
$PbTiO_3$	Lead Titanate
PDMS	Polydimethylsiloxane
PEDOT: PSS	Poly(3,4-Ethylenedioxythiophene) Polystyrene Sulfonate
PAN	Polyacrylonitrile
$ImCLO_4$	Imidazolium Perchlorate
BC	Bacterial Cellulose
BMP	Beats Per Minute
SIDS	Sudden Infant Death Syndrome
COPD	Chronic Obstructive Pulmonary Disease

Chapter 1:
INTRODUCTION

Disclaimer: This chapter (1) is adapted from the following articles with permissions of all co-authors and journal:

Ali, Mohsin, et al. "A Flexible and Biodegradable Piezoelectric-Based Wearable Sensor for Non-Invasive Monitoring of Dynamic Human Motions and Physiological Signals." Advanced Materials Technologies: 2300347.

Ali, Mohsin, et al. "Biodegradable Piezoelectric Polymers: Recent Advancements in Materials and Applications." Advanced Healthcare Materials (2023): 2300318.

My contribution: conceptualization, design, fabrication, experiments, figures, and writing.

This chapter aims to mark the problems to be addressed and the challenges behind the aims of this thesis. First, an overview of piezoelectric materials and their application is introduced, followed by presenting the recent advancements in bioresorbabale piezoelectric. Last, strategy for the fabrication of novel biodegradable piezoelectric polymer and its integration to fabricate a flexible wearable piezoelectric sensor using easy and simple fabrication process.

Piezoelectricity is the ability to convert applied stress to electric current enabled by a specific material.[1,2] Generally, piezoelectric materials generate charges on two opposite surfaces in response to different mechanical deformation modes such as bending, stretching, and twisting. The unique feature of piezoelectric materials is their non-symmetric crystal structure that allows aligning the opposite ions to form an electric dipole moment. These dipole moments are uniformly oriented in the crystal regions that create domain structures. Upon exposing the material to an external electrical field, the domain orientation will be aligned in a single direction leading to overall uniform polarization of the material and intensifying the piezoelectric response.[3] Once piezoelectric materials are subjected to external stress, the material is polarized along the stress direction, which releases charges in the material, known as direct piezoelectricity.[4]

The application of piezoelectric materials has been investigated in sensation and actuation[5] for developing energy harvesters,[6] electronic skin,[7] smart textiles,[8] and biomedical devices (**Figure 1.1**).[9] Representative piezoelectric materials are inorganic ceramics such as lead zirconium titanate (PZT), barium titanate ($BaTiO_3$), potassium sodium niobate (KNN), bismuth-sodium titanate (BNT), and lithium niobate ($LiNbO_3$). However, there are significant concerns regarding the biocompatibility and biosafety of conventional piezoelectric materials that can raise electronic waste (E-waste) or induce toxicity in host tissue in the case of implantable medical devices (IMDs). There are two main drawbacks to using lead-based piezoelectrics, such as the brittleness of these ceramics and the toxicity of the lead element.[10] Alternatively, lead-free piezoelectrics have been developed, such as $BaTiO_3$ and KNN; however, the electrical properties of KNN are susceptible to temperature, or BNT has a large hysteresis.[11] Besides, the $BaTiO_3$ has a low Curie temperature, limiting its potential applications.[12] Polyvinylidene fluoride (PVDF) and its copolymers as flexible organic piezoelectrics are some alternatives to ceramic-based inorganic piezoelectrics.[13] However, the major drawback of PVDF is the HF (heart failure) remnants by its degradation, an ultra-toxic acid molecule dangerous to the environment and human life.[14]

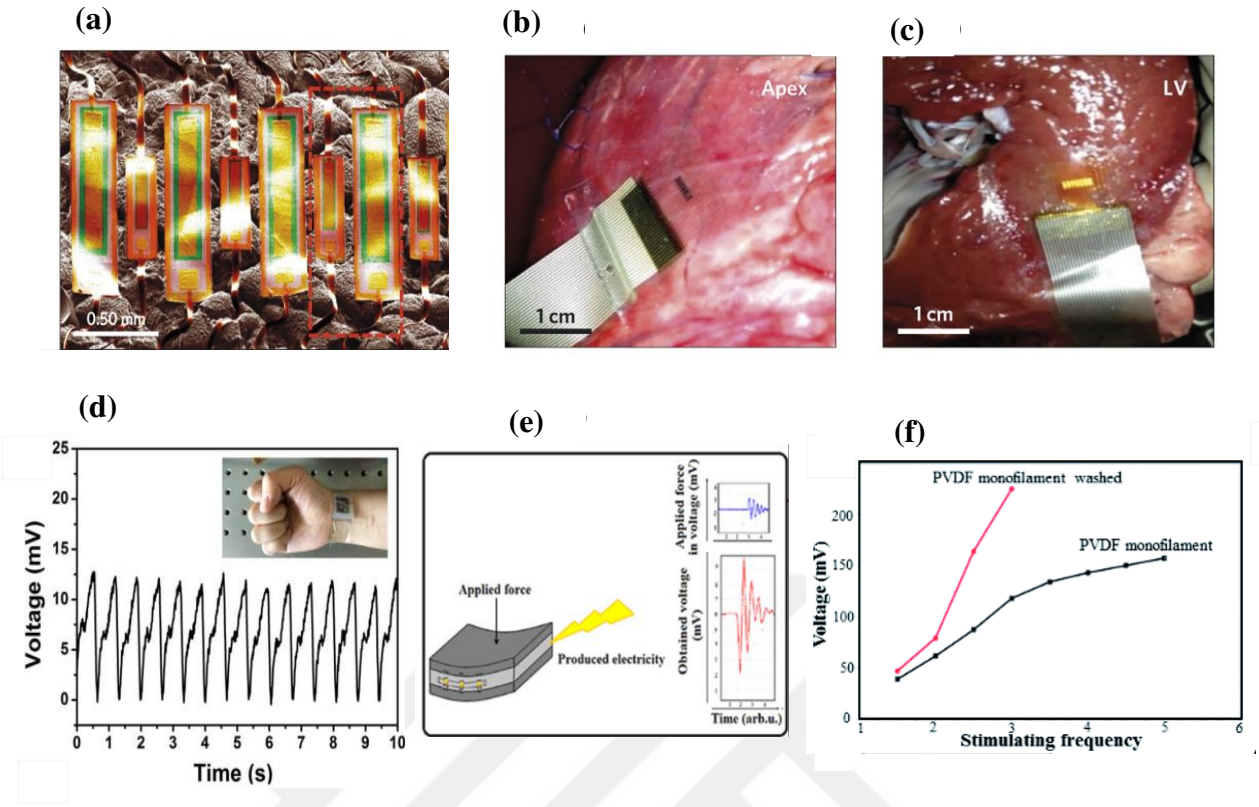

Figure 1-1: ***Applications of common piezoelectric materials***. *(a) Sensor and actuator assembly based on PZT for in vivo measurements of soft tissue viscoelasticity in (b) heart apex, (c) left ventricle. Reused with permission.*[26] *Copyright, 2015. Nature. (d) PVDF-TrFE based piezoelectric pressure sensor utilized for the monitoring of heart rate from radial artery.*[226] *Reused with permission. Copyright, 2018. National library of medicine. (e) A flexible pressure sensor based on PZT and PVDF composite for energy harvesting applications. Reproduced with permission.*[227] *Copyright, 2020. Elsevier. Washability of PVDF based smart textile. (f) Voltage output before and after washing PVDF nanofilaments. Reproduced with permission.*[228] *Copyright, 2018. Royal society of chemistry.*

In recent years, with the advent of biodegradable piezoelectric materials, there has been an opportunity to alleviate e-waste concerns and improve the biocompatibility of the devices. This category of materials can be utilized to develop implantable medical devices that can perform over a specific timespan in a body environment. Subsequently, they will be absorbed in bodily fluids or degraded to harmless units that eliminate the need for retrieval surgery.[15]

Biodegradable piezoelectric polymers are classified as naturally and synthetically driven polymers. Collagen is one of the natural piezoelectric materials, a soft tissue that

mainly contributes to the piezoelectricity of the bone in the human body.[16–18] On the other hand, natural piezoelectric materials can be found in nature. For instance, wood is another raw piezoelectric material due to the presence of cellulose in its structure.[19–21] Poly(l-lactic acid) (PLLA) is one of the synthetically derived biodegradable piezoelectric polymers synthesized by the polymerization of l-lactic acid monomers. The piezoelectric functionality of PLLA is demonstrated as a force sensor in the literature.[22] Even though these biodegradable piezoelectric materials have lower piezoelectricity than ceramic-based ones, several approaches can be applied to enhance their piezoelectricity, such as by modifying their crystal structures.[23–25]

Recognition of instantaneous physiological signals through real-time health monitoring enabled by biomedical devices is receiving significant attention in daily life.[26–28] Biomedical wearable devices as conformal skin-mountable forms are utilized in personalized health care.[29] High-accuracy monitoring of human behavioural patterns and physiological signals [30,31] in addition to the body motions[32,33] are feasible through the seamless integration of the device with the skin of the human body. In this way, several biomedical devices have been demonstrated with various working principles, including electrostatic, piezoelectric, capacitive, and piezoresistive effects.[34–36]

A variety of flexible pressure sensors based on capacitive[37–39] and piezoresistive[40,41] mechanisms have been widely studied for measuring the physiological signals generated by human activities. However, supplying voltage to operate these devices is considered a crucial barrier to the development of energy-efficient wearable sensors.[42,43] Additionally, frequent replacement of the power source limits the application of wearable and implantable electronics for both in vivo and in vitro environments.[44] As an alternative, a self-powered pressure sensor is deemed an appropriate contender to resolve the issue related to power consumption for future wearable healthcare sensors. In this sense, pressure sensors based on piezoelectric[45,46] and triboelectric effects [47–49] can directly produce electricity with external force, enabling the realization of a self-operating sensor. Triboelectric-based devices operate based on the triboelectric effect and electrostatic induction. However, the triboelectric sensor has some downsides including vulnerability to humidity, limited detection of bio-signals, complex fabrication, and abrasion resistance.[50,51] To this extent, devices based on the piezoelectric effect hold top-notch promise in advanced human-machine interface

(HMI) devices compared to other devices owing to the various advantages, including self-powered ability, high sensitivity, and facile fabrication.

Piezoelectric polymers have been reported to manufacture transducers and force/pressure sensors.[52,53] Yuan et al. fabricated a composite piezoelectric material based on poly (vinylidene fluoride) (PVDF) and ZnO to detect human elbow flexure.[7] PVDF is the most commonly used flexible and piezoelectric polymer demonstrating high piezoelectricity compared to other piezoelectric polymers.[54] However, it is not suitable to use as eco-friendly material because it contains non-degradable components[55] and waste produced by these materials is considered as a threat to our environment. Additionally, the polarization of such material is necessary to maximize the piezoelectricity that requires high-temperature annealing and an electric poling process.[56] Such conditions make it challenging to develop flexible biodegradable sensors on bendable/flexible substrates for healthcare applications.[57,58] Emerging innovations in wearable health monitoring systems require the fabrication of self-powered biodegradable devices to monitor the physiological state of the human body.[38,59] For example, pressure sensors placed under the compression bandage could be effective, and their bio decomposition is needed for hygiene purposes. Investigating this aspect, the demand for new biodegradable piezoelectric materials is progressively becoming important for wearable sensors.

Natural biodegradable and biocompatible piezoelectric materials such as peptide nanotubes, cellulose, collagen, and amino acids have augmented significant interest.[60–62] On the other hand, the low stability and irregular arrangements of natural biodegradable piezo materials [63] have limited their use in real-time applications. Thus, due to the weak macro-scale piezoelectric response, most naturally driven materials exhibit nonuniform piezoelectricity. Although biodegradable glycine-based amino acids have recently been reported with a high piezoelectric coefficient,[64] fabricating functional films with controllable piezoelectricity from these powder-based materials is challenging.

In the case of a synthetically biodegradable piezoelectric polymer, Poly (L-lactide acid) (PLLA) is attracting attention because of its excellent biocompatibility and biodegradability in biomedical devices such as FDA-approved implants and biodegradable force sensors.[65–70] Although PLLA exhibits modest piezoelectricity (5-15 pC/N) and has a low dielectric constant, it provides energy conversion efficacy like commercial piezoelectric polymer PVDF.[66,71] PLLA-based piezoelectric devices have

been used in bio-applications, such as filtration devices, smart fabric, pressure sensors, and actuators.[72–74] Polymerization of l-lactide monomers results in the formation of PLLA.[72] The molecular chain of PLLA comprises chiral molecules where the carbon-oxygen double bond is connected to an asymmetric carbon atom and displays helical conformity in the molecules. Slight rotation in C=O results in polarization of the chain molecule.[68,75] Polarization occurs when the stress is applied perpendicularly to the plane, resulting in electric Polarization.[65,68] The α-crystalline form of PLLA is thermodynamically stable where C=O dipoles are randomly positioned by the side of the main chain, resulting in no polarization. In order to generate piezoelectricity, the α-form of PLLA must be converted to β-crystalline form where the molecular chains are more aligned.[76] Curry et al. thermally stretched bulk PLLA films to generate piezoelectricity. However, some problems were observed, like complex film processing, film rigidity and low reproducibility,[77,78] which makes stretched piezo PLLA film inappropriate for sensitive pressure sensors, transducers, and actuators.

The motivation of this work is to overcome the challenges mentioned above. A flexible, biodegradable, stretching-free piezoelectric film with a stable piezoelectric response is needed that can be facilely fabricated and has a high potential to be implemented in various sensing applications.

1.1 This work

Herein, we present a strategy for the development of biodegradable, flexible, stretching-free, and cost-effective film with efficient, stable, and controllable piezoelectric film fabricated based on PLLA/glycine. We introduced a new method of inducing the piezoelectricity in biodegradable PLLA polymer by incorporating a specific amount of glycine amino acid. Glycine amino acid incorporated as a nucleating agent which remarkably increased the crystallization rate and degree of crystallinity of PLLA.[79–85] The amount of glycine is optimized to increase the crystallinity of PLLA. After the development of biodegradable piezoelectric material (PLLA/Gly), we demonstrate the self-powered wearable device constructed based on self-power biodegradable piezoelectric material. Additionally, an assessment of film's piezoelectricity is conducted to show the capability of bioresorbable piezoelectric film for real-time health monitoring applications. Subsequently, we demonstrate that the sensor detected non-invasive human

physiological signals. We also show the biodegradability of piezoelectric PLLA/Gly film in PBS at 37 °C. Despite several accomplishments in the field of biodegradable electronics[38,86,87], this study introduces an easy-to-fabricate, flexible, highly efficient, and biodegradable piezoelectric material, which is only made of bioresorbable materials used for medical applications. The newly fabricated bioresorbable piezoelectric material could be a potential candidate for fabricating implantable sensing devices if used with biodegradable electrodes.

1.2 Thesis outline

In chapter 2, we will thoroughly cover the most recent literature regarding natural and synthetic bioresorbable piezoelectric materials. In chapter 3, fabrication and characterization methods will be discussed. Result and discussion will be covered in chapter 4. The thesis will end with a conclusion section in chapter 5.

Chapter 2:
LITERATURE REVIEW

Disclaimer: This chapter (1) is adapted from the following articles with permissions of all co-authors and journal:
Ali, Mohsin, et al. "A Flexible and Biodegradable Piezoelectric-Based Wearable Sensor for Non-Invasive Monitoring of Dynamic Human Motions and Physiological Signals." Advanced Materials Technologies: 2300347.
Ali, Mohsin, et al. "Biodegradable Piezoelectric Polymers: Recent Advancements in Materials and Applications." Advanced Healthcare Materials (2023): 2300318.
My contribution: conceptualization, design, fabrication, experiments, figures, and writing.

This chapter aims to address the significant and recent advancements in biodegradable piezoelectric materials, including natural and synthetic polymers. An overview of natural and synthetic biodegradable piezoelectric materials used for fabricating various biomedical devices.

2.1 Natural Biodegradable Piezoelectric Polymers

Nature can be considered the origin of piezoelectricity. Traces of piezoelectric materials could be found from the living cells and tissues to the jungles and seashores. The piezoelectricity in nature-derived materials was first recognized by using viruses,[63] fish bladders,[88] and prawn shells[89] as piezoelectric generators in electric circuits. Since then, research on organic piezoelectric biodegradable materials has grown considerably. Naturally driven materials possess well-organized structures with low inversion centers and symmetry. Therefore, several biological materials show the inherent ability of linear electromechanical coupling. Since the investigation of piezoelectricity in natural biodegradable materials like collagen,[90] chitin,[91] and cellulose,[90] many bio-based materials have been observed to produce piezoelectricity. Organic biological materials, including small amino acids, proteins, peptides, and polysaccharides with chiral crystal symmetry to the giant hierarchical molecules of biomaterials, featured helical and fibrous structures with low symmetry.[92] In this section, we will have a comprehensive discussion about these materials.

2.1.1 Proteins and their derivatives

Amino acids are small monomers that act as building blocks of protein structure. These monomers have different functional groups, such as carboxyl (-COOH), amine (-NH_2), and amide. Many studies have reported using protein and its derivatives to fabricate piezoelectric-based devices. Vasilescu et al.[93] conducted the first experiments to find piezoelectric properties in amino acid crystal structures. In this study, different structures like right-handed (D-Alanine) and left-handed (L-Alanine) “racemic” mixture (DL-Alanine) of D and L amino acid structures were investigated. They discovered the piezoelectric property in many of them except those samples with an anonymous crystal structure. Following the decades, in 2000, Lemanov et al. revealed that the piezoelectricity of amino acids depends on the temperature. Additionally, they reported that the piezoelectricity of γ-glycine and DL-alanine is approaching the value for quartz crystals or even higher.[94–97]

Glycine is the only amino acid with a non-chiral structure. It has three crystal polymorphs known as α-glycine, ß-glycine, and γ-glycine. Okosun et al.[98] studied the

repeatable piezoelectric response of films made of glycine/copper under multiple cycles of bending. **Figure 2.1**a and **2.1**b depict glycine/copper film in bending form and an enlarged view of the device displaying copper tape containing an active layer of flexible polycrystalline. Ensieh et al.[99] developed a biodegradable piezoelectric device for measuring pressure based on a chitosan/ß-glycine composite. **Figure 2.1**c shows the optical photographs of free-standing CS/Gly film (c-i) and both film (c-ii) and stretchable sensor (c-iii) deposited on a gold electrode. Guerin et al.'s studies and calculations proved that the anti-parallel molecular dipole in the α-glycine crystal structure, which has the space group of $P2_1/C$, leaves no piezoelectricity for this polymorph by canceling net polarization. On the other hand, ß-glycine and γ-glycine have considerable piezoelectric properties. ß-glycine and γ-glycine structures have the space group of $P2_1$ and $P3_1$, which has the piezoelectric coefficient corresponding to d_{22} and d_{33}. Guerin et al. calculated the d_{33} constant for the γ-glycine, and 10.4 pm V^{-1} was reported. The coefficient of shear piezoelectricity, d_{16}, was anticipated to be 195 pm V^{-1} in the ß-glycine phase, which was then verified experimentally through an impedance analyzer and piezometer. Also, they measured the d_{16} coefficient in ß-glycine around 178 pm V^{-1}, which turned out close to the coefficients magnitudes of BTO[100] and KNN.[101] Although amino acids' piezoelectric performances are outstanding, their functionality is not sustainable due to their metastable structure.[102,103]

The ferroelectric phenomenon was also observed in glycine. Several biomaterials exhibit piezoelectric properties, but ferroelectricity is relatively rare. Somewhat differing from this statement, many ferroelectric materials are partly organic. For instance, triglycine sulfate ($(NH_2CH_2COOH)_3. H_2SO_4$) (TGS) is perhaps the most researched.[104] The control of polarization direction upon applying an electric field in biomolecules is known as bio-ferroelectricity.[105][106] It is well-considered that ferroelectricity is in close relation with piezoelectricity. However, the biological importance of bio-ferroelectricity is not poorly assumed. Recently, strong ferroelectricity was found in croconic acid crystal, exhibiting a spontaneous polarization nearly equal to barium titanate (~ 20 μC cm^{-2}) at room temperature.[107] This provoked a new wave of attraction towards low molecular weight organic materials.

Recently, ferroelectricity was observed in the β and γ-form crystals of the glycine, and it is likely to use an external electric field to control the polarization direction.[108][109] The third polymorph of glycine, i.e., γ-glycine, is reported as uniaxial, strong

piezoelectric,[110] but ferroelectricity and pyroelectricity in this organic compound have not been observed thus far. Heredia et al.[62] stated for the first time that the γ-form of glycine crystal, which shows piezoelectricity, is also a ferroelectric material. Molecular dynamics and density functional theory (DFT) simulations were used to interpret the sources of ferroelectricity in γ-glycine. This study revealed that the small size of glycine molecules results in the realization of very small polarization bits possibly being applicable, i.e., for the storage of ultra-dense information, which is inherently not possible with common ferroelectrics. Bystrov et al.[108] reported the generation of ferroelectricity in β and γ-glycine and found out that β-glycine exhibit better ferroelectric properties compared to γ-glycine. Both forms of glycine crystals have the same molecular volume. However, γ-glycine has shown stronger and more controlled polarization than β -glycine, as it has dipoles in different directions, whereas γ-glycine has spirally oriented dipoles along the axis. These properties of glycine open up an exciting application for bioelectronics logic, sensors, optics, memory devices, and energy generation.

Another amino acid with significant piezoelectricity is DL-alanine, represented by the D and L-alanine racemic mixtures. First, Lemanov et al.[97] confirmed the piezoelectric property of DL-alanine by transmitting high-frequency electrical pulses on a single crystal of DL-Alanine. Subsequently, Guerin et al.[111] utilized density functional theory (DFT) to predict the piezoelectric tensors of DL-alanine. The DL-alanine piezoelectric coefficient was fabricated by drop-casting their crystals on the Cu substrate, and the film was demonstrated as an energy generator through compression. In another study, they have grown racemic amino acid films on copper electrodes to produce energy. The DL-alanine piezo film was manually compressed between electrodes to get the piezoelectricity **(Figure 2.1**d). The highest measured value of the longitudinal coefficient (d_{33}) was 4.8 pC N^{-1}. This value was comparable to ZnO and aluminum nitride (AlN) coefficients. Finally, Guerin et al. demonstrated that the DL-alanine piezoelectric crystals could be used as biosensors, energy harvesters, and electronic devices.

Another naturally driven biodegradable piezoelectrics are peptides comprised of amino acid building blocks. Diphenylalanine (FF) is one of the peptides formed by the bond of two alanines-a natural amino acid; it has recently attracted attention due to its outstanding piezoelectricity and mechanical properties in addition to its environment-friendly structure. The FFs are self-assembled structures by hydrogen bonding and π-π stacking, particularly in nanotubes.[112–114] In 2010, Kholkin et al. synthesized the FF

nanotubes with a strong shear piezoelectric value, measured by piezoelectric force microscopy (PFM) for the first time.[115] These nanotubes have a hexagonal crystal structure (P_6) that contributes to its magnificent shear piezoelectric response (d_{15}) alongside the tube axis. In another study by Vasiliev et al.[112], d_{33}, d_{31}, d_{14}, and d_{15} coefficients of FF microtubes were measured based on their crystal structure. FF micro-ribbons were fabricated with an orthorhombic shape utilizing inkjet printing and ethylene glycol as solvent by Safaryan et al.[116] It was reported that the coefficient of piezoelectricity d_{15} for orthorhombic FF was around 40 pm V^{-1} by piezo force microscopy (PFM), which was greater than the typically used PVDF polymer. To confirm piezoelectricity in longitudinal mode, a sweep of AC voltage from 0 to 5 V was applied through the tip of PFM placed on hexagonal PNT. A voltage amplitude and displacement slope attributed to d_{33} were calculated at around 18 pm V^{-1}.[112] Other studies reported the d_{33} coefficient of piezoelectricity for FF nanotubes between 9.9 – 17.9 pm V^{-1}.[60,113,117] The measured coefficients stronger response compared to conventional piezoelectric materials. Tao et al.[118] reported a bioresorbable piezoelectric nanogenerator (PENG) by embedding diphenylalanine micro rods into the free-standing film of PLA (**Figure 2.1**e). The fabricated PENG generated a power output of 1.56 $W.m^{-3}$ and an output voltage of 1.76 V. In addition, the device was fully dissolved in phosphate-buffer saline solution, acidic solution, and alkaline solution after 25 days at 60 ºC. Kim et al.[119] fabricated piezoelectric nanogenerator device utilizing diphenylalanine (FF) and tetra(p-hydroxyphenyl) porphyrin (THPP) (**Figure 2.1**f). The fabricated device exhibited a piezoelectric coefficient of $d_{15} \approx 60$ pm.V^{-1} for FF/THPP nanostructures. The resultant piezoelectric nanogenerators can consistently generate the maximum voltage and current density of 2.6 V and 5.8 μA/cm^2, respectively, upon 20 N force exertion. In another study, Park et al.[120] investigated the functionality of diphenylalanine (FF) peptide nanotube-based piezoelectric nanogenerators. The large-scale aligned and unpolarized FF nano-tubes were fabricated using self-assembly methods in different solvent systems. Their optimization results for the alignment of FF nanotubes showed that in ethanol/DI water (75/25) solvent ratio and concentration of 0.4 mg ml^{-1}, the nanotubes exhibited the highest density and uniform alignment at a pulling speed of 20 μm min^{-1}. Regarding the electrical performance of the FF nanotubes-based nanogenerators demonstrated the maximum voltage, current, and power output of 1.66 V, 18.4 nA, and 19.2 nW, respectively, and were stable for more than 3,500 cycles.

The orthorhombic form of FF tubes also exhibited ferroelectric-like behavior after the heat treatment. Only half the polarization switching was observed due to the high coercive field when an external electric field was applied.[121–124] Leuchtag et al.[125,126] observed ferroelectric properties with large values of easily switchable polarization and dielectric permittivity[127,128] in branched-chain homopeptide amino acids such as valine (V), Leucine (L) and isoleucine (I).

Natural proteins have unsymmetrical crystal structures. They have the preliminary eligibility for having piezoelectric responses and consist of piezoelectric amino acid blocks. However, their piezoelectric intensity is low in comparison with other materials. Stapleton et al.[129] measured the piezoelectric property of lysozyme. The highest d_{33} coefficient (~ 6.5 pm V^{-1}) belonged to tetragonal aggregated films of lysozymes.

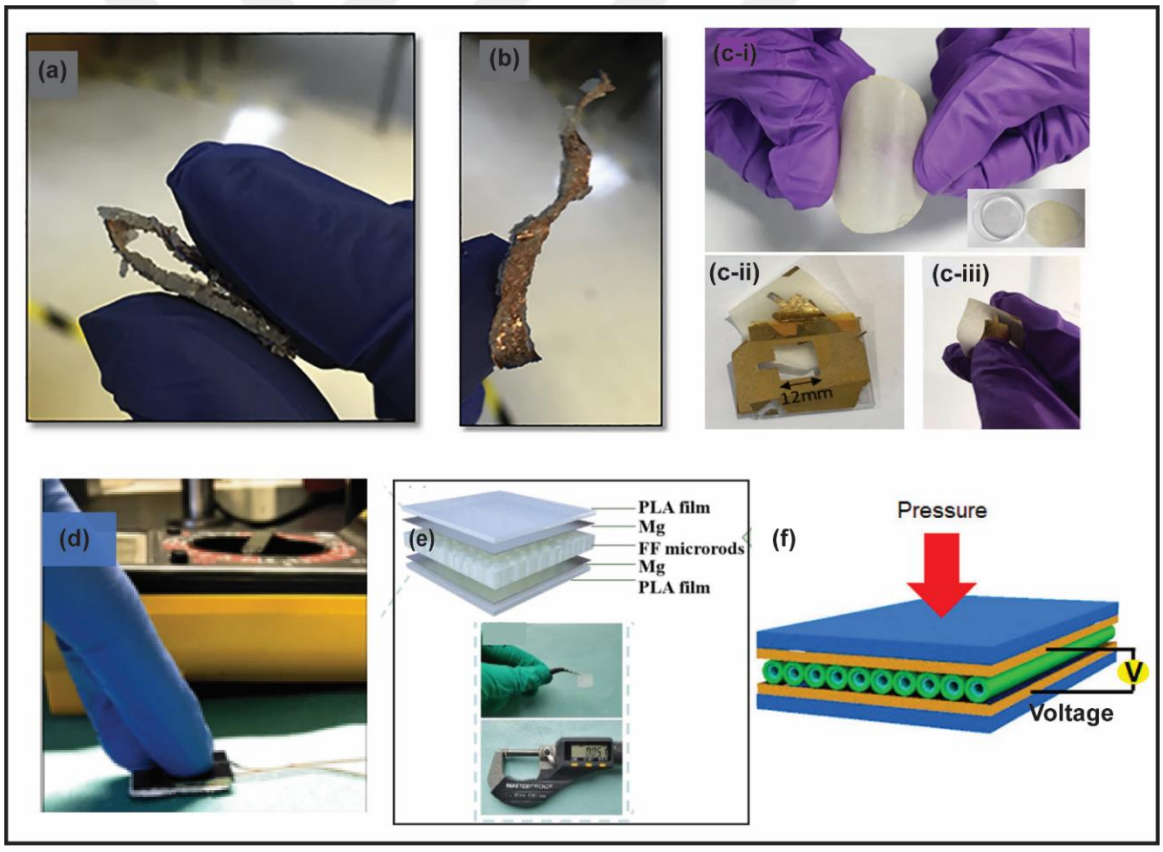

Figure 2-1.1***: Protein and its derivatives-based devices.*** *(a) A completely bent flexible device based on glycine. (b) A view of the full-length flexible device with copper electrodes. Reused with permission.*[98] *Copyright 2021, Elsevier. (c) i- Chitosan/Glycine film peeled off from petri dish. ii-Gold electrode deposited on both sides. iii- Cs/Gly-based flexible sensor. Reproduced with permission.*[99] *Copyright 2020, American Chemical Society. (d) Generation of the output voltage by manually compressing the DL-Alanine film test. Reproduced with permission.*[111] *Copyright 2019, American Physical Society. (e) Schematic of degradable piezoelectric nanogenerator device based on FF nanorods. Reused with permission.*[118] *Copyright 2021, Elsevier. (f) Schematic representation of piezoelectric nanogenerator (PENG) fabricated by utilizing diphenylalanine (FF) nanotubes and porphyrin nanocomposite. Reproduced with permission.*[119] *Copyright 2022, American Chemical Society.*

2.1.2 Polysaccharide

Cellulose is one of the most common varieties of biopolymers. It is a linear polysaccharide, including glucose as the repeated unit, and its intrinsic crystalline structure enables piezoelectrical properties. Plant-based biomass (cellulosic) is the most abundant organic, recyclable raw material available on earth and is universally reproduced by nature via a photosynthetic chemical reaction.[130] Cellulose, a major component of wood, lignocellulosic materials, and agriculture biomass residue, has also been investigated for its piezoelectric properties.[131,132] The small wood piezoelectricity in cellulose was an initial idea to study its piezoelectricity resource.[20] The piezoelectricity accounts for hydrogen bonding between the polysaccharide chains in the cellulosic materials.[133] The widely used cellulosic materials demonstrated to show piezoelectricity are cellulose nanocrystals (CNC), cellulose nanofibers (CNF), and bacterial nano cellulosic obtained from onion skin and bleached birch cellulose.[134–137] This variety of cellulose has two polymorphs, triclinic I_{α} and monoclinic $I_{ß,}$ and both show piezoelectric responses due to the non-symmetric structure of their crystals.[138] However, the piezoelectricity in longitudinal and shear orientation is less than 1 pc N^{-1}.[139]

Rich cellulosic fibers in citrus fruit's wastes (biomass), along with essential oils, flavonoids, and proteins, present piezoelectric properties. Incorporating orange peel powder into the host matrix of PVDF (up to 40 wt%) resulted in the enhancement of piezo phases (by 70%).[140] The piezoelectric nanogenerator (PENG) developed utilizing orange peel-added PVDF paper offered a power density of 135 μWcm^{-2} and an output voltage of 90 V in response to human motions. Maiti et al.[141] fabricated a piezoelectric nanogenerator device based on onion skin (OS) as piezoelectric material. An OS piezoelectric nanogenerator device is illustrated in **Figure 2.2**a. Optical photographs of OS show good flexibility of onion skin in bending, rolling, and twisting modes. A study by Sun et al.[19] reported a low-cost, biodegradable wood sponge-based piezoelectric nanogenerator fabricated through a simple delignification process. The maximum voltage and current outputs were 0.69 V and 7.1 nA, respectively, upon applying a 13 kPa pressure level. The mechanical performance of the sponge wood demonstrated excellent compressibility, improving the piezoelectric properties up to 85 times compared to native timber. In a study about 2D $I_ß$ polymorph, Garcia et al.[133] demonstrated that hydrogen bonding is highly responsible for cellulose piezoelectricity due to its asymmetry and polarization between and within chains. To improve the piezoelectricity of cellulose nanocrystal (CNC) films, Miao et al.[142] prepared hydrolyzed CNCs with acid to generate hydrogen bonds on their surface. These surface-modified CNCs composited with Polyethylene oxide (PEO) showed the maximum piezoelectric response of 23 pC N^{-1} (**Figure 2.2**b). Cellulose nanofibers (CNF) were also observed, showing ferroelectricity. CNF exhibits small remanence polarization generation upon applying an electric field above ~40 V/µm. Rajala et al.[143] reported that CNF films require high voltage application (~40 V/µm) to show ferroelectric characteristics.[144]

Chitin is another category of polysaccharide, one of the components of crustaceans' mushroom cell walls and exoskeletons. It is the second most abundant polysaccharide in the world. It has two distinct polymorphs, α and ß Chitin.[145] In the early 1970s, Fukada et al.[91] found the shear piezoelectricity in the α-chitin. In a recent study, Kim et al.[146] fabricated a biodegradable piezoelectric film made of chitin nanofibers showing good performance and functionality as a flexible piezoelectric device **(Figure 2.2**c**).** The piezoelectricity coefficient of the ß-Chitin nanofibrous film was measured at 4 pm V^{-1}, which agrees with their DFT calculations. Hoque et al.[147] utilized biowaste obtained from crab shells to extract chitin nanofibers. The chitin nanofibers fabricated a thin film

piezoelectric nanogenerator with an excellent piezoelectric response. The piezoelectric nanogenerator generated an output voltage of 22 V and short circuit current (I_{sc}) = 0.12 μA

Chitosan is also a natural polysaccharide that can be extracted from chitin deacetylation. This linear polysaccharide is composed of β-1,4-D-glucosamine.[148] Chitosan has an orthorhombic structure with a nonsymmetric space group of $P2_12_12_1$, and thus it shows the piezoelectric property.[149] Owing to its straightforward water-based solution processing, biodegradability, biocompatibility, low cost, and availability of renewable raw material sources, it is being used in numerous applications.[150–153] A recent study reported the generation of piezoelectricity using chitosan extracted from fungal biomass. Chitosan derived from the fungal biomass showed great potential for utilizing an ecological source of chitosan to fabricate piezoelectric thin films of chitosan.[154] Chitosan has drawn significant attention in research areas including biodegradable sensors and energy harvesters. Such applications are based on the effect of piezoelectricity generated by these materials, which means they can develop electrical charges under mechanical stress.[155] In the preliminary study, the piezoelectric sensitivity of chitosan has been reported [156] as well as in the current study, a vibration sensor based on piezoelectricity of chitosan was developed.[157] The maximum d_{33} coefficient of chitosan reported in this study was 18.4 pC N^{-1}.[157]

2.1.3 Animal-derived piezoelectrics

The most common biodegradable piezoelectric polymer in the animal and human body is collagen. This has a ubiquitous presence inside the organs and tissues.[158] In addition to the bone tissue, other collagen-contained tissues like cartilage, ligament hair, and skin can exhibit piezoelectric properties.[7,159–161] Although there is no proven theory about the piezoelectricity mechanism in collagen, a standard theory suggests that piezoelectricity in each polypeptide chain of the collagen is related to the charge dipole corresponding to the amine (N)-carboxyl (C) bound of two ends of amino acids in the one collagen molecule.[18,162] Ghosh et al.[163] fabricated an energy harvesting device utilizing fish skin (collagen) as biodegradable piezoelectric materials. **Figure 2.2**d depicts the

fabrication method of a fish skin (biomass) based nanogenerator. The developed flexible device acted as a sensor for monitoring physiological signals such as radial artery pulse rate and joint motion (**Figure 2.2**e). Vivekananthan et al. [164] developed a piezoelectric nanogenerator device having dimensions 3 cm x 3 cm by utilizing active layers of collagen (**Figure 2.2**f).

Some studies have been conducted to reveal the piezoelectric coefficient of collagen recently. For instance, Denning et al.[165] they measured the d_{14} = 12 pm V^{-14} in the fibrillary rat tail collagen via PFM, showing the highest piezo response from the neat collagen. In another study, Zhou et al.[166] studied the molecular mechanism of collagen piezoelectricity based on the twisted collagen model. Their experiments and calculations contributed to understanding the origin of polarization from polar and charged groups in the molecule. In addition, the mechanical stress can change and reorient the dipoles and hence, the magnitude of piezoelectricity. Methods and processes can be applied to create high piezo-responsive systems to enhance the collagen structure's piezoelectricity. Nair et al.[167] made the collagen bundles with self-assembly and by cross-linking them utilizing three crosslinking agents, EDC-NHS (A solution based on 1-ethyl-3-(3-dimethyl aminopropyl) carbodiimide hydrochloride and N-hydroxysuccinimide), genipin, and tissue transglutaminase. These three agents enhanced the vertical piezoelectric response of collagen bundles. In another recent work by Bera et al.[168], they assembled collagen-mimicked tri-peptide structures from short peptide sequences. The resulting peptide chain has a helical structure like collagen, and its d_{35} coefficient reached 27 pm V^{-1} thanks to introducing the hydroxyl group.

Silk, an animal-derived material, could be obtained as silk fibroins (SF) from Bombyx mori cocoons or spider silk (SS) from spiders. The silk gains its piezoelectric response from the α-helix and ß-sheet substructures inside its structure.[169,170] Yucel et al.[171] prepared the SF films via a solution drying and consequent draw method. They found that the piezoelectric property of SFs is obtained from ß-sheet generation and uniaxial molecular direction. The shear piezoelectricity property was enhanced by increasing ß-sheet content and crystallinity. The ß-sheet increase resulted from zone drawing of SF films. Therefore, mechanical treatment would be considered a way to increase piezoelectricity in silk. Chiesa et al.[172] introduced biodegradable piezoelectric with soft and holey structures based on 3D-printable silk material for monitoring soft tissues in vivo (**Figure 2.2**g). Furthermore, Pan et al.[173] designed a repolarization

process for improving the piezoelectricity in the silk fibers. They increase the piezoelectric response of SS fibers from 13.4 to 40.7 mV, thanks to the rearrangement of fibers more orderly manner. Silk was also observed to exhibit ferroelectric behavior. Sencadas et al.[174] reported with the help of PFM results that electrospun and methyl alcohol-treated silk samples show the features of ferroelectric materials. In addition, when electrospun silk fibers were submitted to methyl alcohol vapor, the polymer chains started aligning in a more oriented fashion, resulting in better ferroelectric response upon high voltage application.

2.1.4 Virus

The M13 phage virus is one of the fascinating biomaterials to mimic biological structures and shows piezoelectric properties. With their filamentous structure clad with helical proteins, these viruses represent a system like human collagen and can mimic its physical properties like piezoelectricity. Due to their phase-changing conformation, highly-ordered crystalline structures can be prepared from the M13 phages.[175] In 2012, Lee et al.[63], was the first group to study the piezoelectricity of M13 phages and the piezoelectric coefficient of M13 phages thin film was measured up to 7.8 pm V^{-1} via PFM. They also showed the capability of tuning the phages' piezoelectric response by engineering the coat proteins of filaments. Heo et al.[176] recently fabricated the morphology-modulated hierarchical structures of M13 phage films. Due to the long-range ordered chiral structures from single phage to the macro-scale band of M13s, the piezoelectrical property of M13 phages was enhanced while used as a power generator in a circuit. In another study, Shin et al.[177] improved the piezoelectrical response of M13 by aligning them vertically. They extruded the phages at various speeds into an anodic aluminum oxide template (AAO) until phages filled it with a porous structure. These vertical phage nanopillars yield a d_{33} coefficient of around 10 pm V^{-1}, proving their versatility in several electronic and bioelectronic applications.

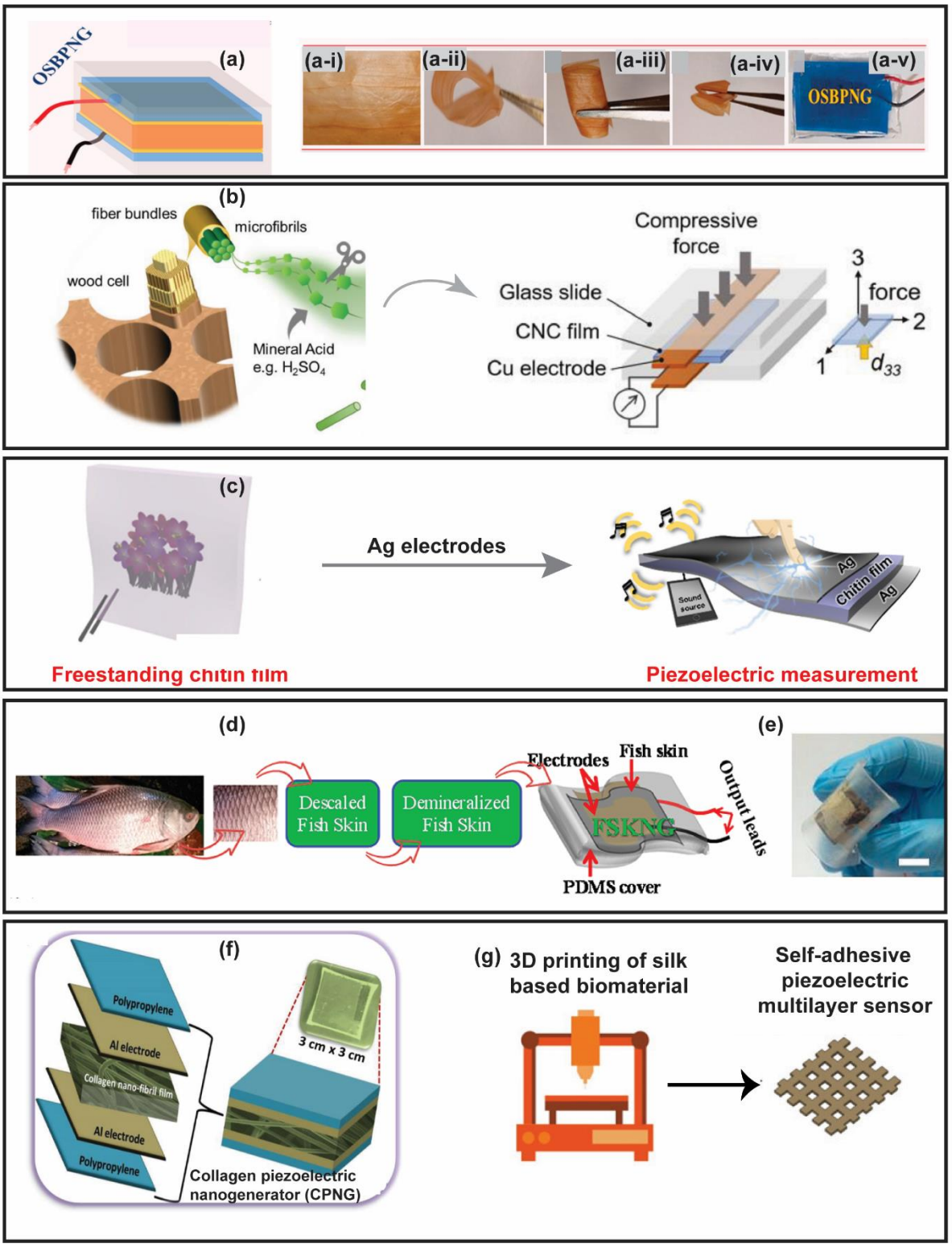
OSBPNG
(a)
(a-i)
(a-ii)
(a-iii)
(a-iv)
(a-v)
OSBPNG
(b)
fiber bundles
microfibrils
wood cell
Mineral Acid
e.g. H_2SO_4
Compressive
force
Glass slide
CNC film
Cu electrode
3
force
2
1
d_{33}
(c)
Ag electrodes
Ag
Chitin film
Ag
Sound source
Freestanding chitin film
Piezoelectric measurement
(d)
Descaled
Fish Skin
Demineralized
Fish Skin
Electrodes
Fish skin
Output leads
FSKNG
PDMS cover
(e)
(f)
Polypropylene
Al electrode
Collagen nano-fibril film
Al electrode
Polypropylene
3 cm x 3 cm
Collagen piezoelectric
nanogenerator (CPNG)
(g) 3D printing of silk
based biomaterial
Self-adhesive
piezoelectric
multilayer sensor

Figure 2-2: *(a) i- Cross section view of onion skin bio piezoelectric nanogenerator ii-film of onion skin iii- bending of onion skin iv- rolling of onion skin and v- twisting of onion skin. Reproduced with permission.*[141] *Copyright 2017, Elsevier. (b) Cellulose nanocrystals derived from wood via sulfuric acid (H_2SO_4) hydrolysis. Schematic of cellulose nanocrystal-based sensor for the measurment of d_{33} (right). Reused with permission.*[142] *Copyright 2021, Elsevier. (c) Piezoelectric transducer device based on chitin (piezoelectric material). Reused with permission.*[146] *Copyright 2018, Elsevier. (d) Demonstration of the fabrication process of a nanogenerator based on fish skin. (e) Optical image of fish skin-based nanogenerator depicting flexibility. Reused with permission.*[163] *Copyright 2017, American Chemical Society. (f) Schematic representation of collagen piezoelectric nanogenerator. Reused with permission.*[164] *Copyright 2018, American Chemical Society. (g) Multilayer piezoelectric sensor fabricated by 3D printing of silk. Reused with permission.*[172] *Copyright 2022, American Chemical Society.*

2.2 Synthetic Biodegradable Piezoelectric Polymers

Besides naturally driven piezoelectric polymers, another class of biodegradable piezoelectric polymers is synthetically developed piezoelectric materials. Polylactic acid (PLA) and poly-L-lactic acid (PLLA) are two main synthetic biodegradable piezoelectric polymers that will be discussed in the next section, in addition to the other novel synthesized piezoelectric biopolymers.

The PLA has unique piezoelectric properties as a replacement for the common inorganic and organic piezoelectric material.[178,179] PLLA is another conformation of PLA containing L stereoisomers**.** The piezoelectricity properties in both PLA and PLLA depend on crystallinity and molecular orientation. These polymers have a semi-crystalline structure with a natural chiral conformation that grants piezoelectricity. The electric dipoles of C=O bonds with an aligned form and branched out of polymer backbone are responsible for piezoelectricity.[180,181] The experiments revealed that the PLLA has piezoelectricity parallel to the z-axis with a d_{14} coefficient of 7-12 pC N^{-1}.[182,183] The stretching treatment in PLA and PLLA can orient the chains and enhance piezoelectricity.

Smith et al.[64] measured the piezoelectric coefficient in the highly oriented nanowires grown in the anodized aluminum oxide (AAO) confined environment. The crystallinity of PLLA nanowires was improved by 70% with the nano-confinement method. In the measurements with the PFM, strong shear piezoelectricity was deflected from lateral signals along the nanowires. This deflection yields the value of d_{14} around 8 pC N^{-1}. Curry et al.[22] fabricated a fully biodegradable piezoelectric sensor made by sandwiching the films of piezoelectric PLLA between molybdenum electrodes (**Figure 2.3**a). They studied the drawing effect on the piezoelectric properties of PLLA. The as-synthesized PLLA film shows three faces of (1 1 1), (2 0 0), and (1 1 0). As the drawing ratio increased, the (1 1 1) plane peak decreased in the PLLA X-ray diffraction (XRD) graph. This is reasoned by the transformation of the α phase of PLLA with the 10_3 helical conformations to the ß phase with the 3_1 helical conformations. The best piezoelectric property was obtained by the drawing ratio of around 2.5 to 4.5. According to this study, it was concluded that the C=O dipoles could align uniaxially by drawing, hence effectively improving the piezoelectricity of PLLA. The alignment of PLLA could also be achieved with the help of electrospinning of aligned nanofibers, resulting in macro piezoelectricity. For instance, Zhu et al.[184] fabricated PLLA porous nanofibrous scaffolds with aligned morphology via melt drawing. They realized the piezoelectricity property in the nanofibers with the size 100 nm and 40 µm. Furthermore, the increase of piezoelectricity was observed with the increase of uniaxial force upon the nanofibers. In another inceptive study, Curry et al.[185] demonstrated a biodegradable device that worked as a force sensor for measuring physiological pressure and an ultrasonic transducer to assist drug delivery and blood-brain barrier opening. The biodegradable device was made of nanofibers of piezoelectric PLLA, PLA encapsulation, and molybdenum electrodes (**Figure 2.3**b). Wu et al.[186] fabricated an ultrasonic-driven biodegradable piezoelectric nanogenerator for sustainable electrical signal transmission. This device consisted of fully biodegradable piezoelectric poly(3-hydroxybutyrate-co-3-hydroxyvalerate) (PHBV)/Poly (lactic acid) (PLLA)/potassium sodium niobate (KNN) as functional layer (**Figure 2.3**c). The voltage and current output levels were increased to 6 V, and 0.5 µA, respectively, by a 50% increase in KNN amount. Yousry et al.[187] developed a conformable shear mode ultrasonic transducer based on bioresorbable piezoelectric PLLA nanofibers. A wide range of frequency (500 kHz) was applied to evaluate the electromechanical responses over the macroscopic area of the transducer. The fabricated biodegradable ultrasonic

transducer showed a high level of sensitivity in detecting imperfections in air and liquid. Further, the developed PLLA does not require electric poling to impart piezoelectricity because the shear mode originates from the chemical structure of PLLA itself. The shear mode ultrasonic transducer based on PLLA shows great potential for underwater structural health monitoring applications. **Figure 2.3**d schematically presents the underwater structural health monitoring technique with the help of ultrasonic shear waves utilizing shear piezoelectric ceramic-based transducers compared with transducers based on shear biodegradable piezoelectric polymers. The shear mode piezoelectric polymer-based transducers contain in-plane mechanical coupling, not needing electrical poling, are low profile and shapes conformal; shear ceramic piezoelectrics are not shaped conformal, needed electrical poling and have a high profile. Zhang et al.[73] demonstrated electrospun-based PDLA/PLLA nanofibers (**Figure 2.3**e, left) that improve filtration efficiencies for removing small particulate matter (PM). The surface charges generated from piezoelectric PLLA membrane (**Figure 2.3**e, right) with controllable porosity demonstrated great improvement in capturing small-sized particles (i.e., PM2.5). Additionally, they demonstrated the fabrication optimization parameters, such as solution concentration and electrospinning time to improve the quality factor, up to 4.6% compared to conventional 3M respirator filters. Le et al.[188] fabricated a highly efficient, recyclable, self-sustaining, and humidity-resistant air filtration membrane utilizing biodegradable PLLA nanofibers with stable piezoelectricity and long-term biodegradability (**Figure 2.3**f). Based on the effect of aeolian vibrations, the self-charged PLLA nanofibers membrane (Figure 4g) permits the joined impact of mechanical sieving, and It increases electrostatic adsorption to eliminate particulate matter (PMs). In the current studies, researchers are developing synthetic biodegradable piezoelectric polymers utilizing natural piezoelectric materials.

For instance, Yang et al.[189] demonstrated a self-assembly-based and wafer-scale approach to fabricate a PVA-glycine-PVA sandwich structure. **Figure 2.3**h depicts the synthesis route of the glycine-PVA-based bioresorbable piezoelectric film. The sandwiched piezoelectric structure exhibited an impressive piezoelectric response (g_{33} = 157.5*10^{-3} Vm/N) comparable to commercial piezoelectric materials such as PVDF-TrFE. The sandwiched piezoelectric structure exhibited an impressive piezoelectric response (g_{33} = 157.5*10^{-3} Vm/N) relative to commercial piezoelectric materials such as PVDF-TrFE.

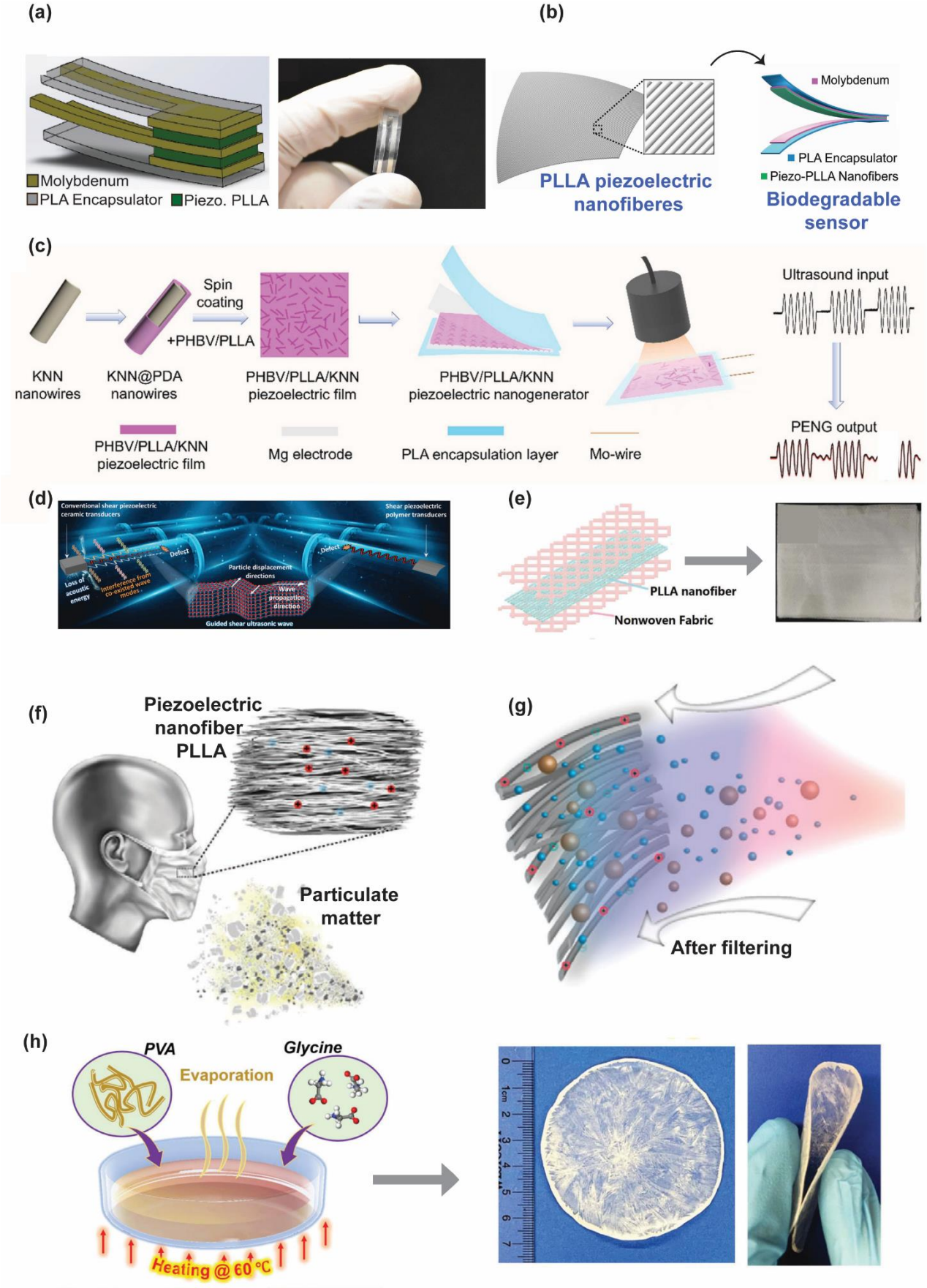
(a)
Molybdenum
PLA Encapsulator
Piezo. PLLA
(b)
PLLA piezoelectric nanofiberes
Molybdenum
PLA Encapsulator
Piezo-PLLA Nanofibers
Biodegradable sensor
(c)
KNN nanowires
KNN@PDA nanowires
Spin coating
+PHBV/PLLA
PHBV/PLLA/KNN piezoelectric film
PHBV/PLLA/KNN piezoelectric nanogenerator
Ultrasound input
PENG output
PHBV/PLLA/KNN piezoelectric film
Mg electrode
PLA encapsulation layer
Mo-wire
(d)
Conventional shear piezoelectric ceramic transducers
Shear piezoelectric polymer transducers
Defect
Particle displacement directions
Wave propagation direction
Guided shear ultrasonic wave
(e)
PLLA nanofiber
Nonwoven Fabric
(f)
Piezoelectric nanofiber PLLA
Particulate matter
(g)
After filtering
(h)
PVA
Glycine
Evaporation
Heating @ 60 °C

Figure 2-3*: Bio-decomposable force sensor based on piezoelectric PLLA. (a) A simple illustration of the piezoelectric and biodegradable sensor (left) and optical photograph of the developed piezoelectric and bio-decomposable sensor (200um thick and 5mm x 5mm) (right). Reproduced with permission.[22] Copyright 2018, Proceedings of National Academy of Science. (b) A simple representation of processed piezoelectric PLLA nanofibers (left) and schematic illustration of the biodegradable pressure sensor (right). Reproduced with permission.*[185] *Copyright 2020, Proceedings of National Academy of Science. (c) Representation of fabrication process of PHBV/PLLA/KNN composite film-based nanogenerator. Reused with permission.*[186] *Copyright 2022, Elsevier. (d) A schematic representation of underwater structural health monitoring technology by guided ultrasonic waves utilizing a shear piezoelectric polymer-based transducer compared to a shear piezoelectric ceramic transducer. Reused with permission.*[187] *Copyright 2023, Wiley. (e) Schematic demonstration of PLLA filter structure (left) and optical image of PLLA filter membrane (right). Reproduced with permission.*[73] *Copyright 2019, Wiley. (f) Concept photograph and schematic illustration of facemask using electrospun biodegradable piezoelectric PLLA nanofibers. (g) The combined influence of mechanical sieving and increased electrostatic adsorption is because of the piezoelectric effect in trapping particles. Reproduced with permission.*[188] *Copyright 2022, Wiley. (h) Schematic representation of the synthesis of PVA-glycine biodegradable piezoelectric films (left). The Right image is the optical image of a wafer-sized grown flexible film. Reproduced with permission.*[189] *Copyright 2021, Science.*

Chapter 3:

MATERIALS AND METHODS

Disclaimer: This chapter (1) is adapted from the following articles with permissions of all co-authors and journal:
Ali, Mohsin, et al. "A Flexible and Biodegradable Piezoelectric-Based Wearable Sensor for Non-Invasive Monitoring of Dynamic Human Motions and Physiological Signals." Advanced Materials Technologies: 2300347.

This chapter aims to provide the details for materials and characterization methods used for this study. Every characterization method

3.1 Flexible piezoelectric PLLA/Gly film preparation:

Poly (L-Lactic Acid) (PLLA) pallets (PURASORB PL24) and glycine utilized in this study were acquired from Corbion (Netherland) and ISO Lab (Germany), respectively. A solution of 5 (wt. %) poly (L-lactic) acid was prepared by dissolving PLLA (PURASORB PL 24) in 1,4 dioxane (Panreac) through magnetic stirring at 80 ^{o}C, followed by stabilizing the solution at room temperature. Then, solution of PLLA/Gly was prepared by incorporating different weight percentages of glycine amino acid as of dry PLLA into the solution of PLLA at room temperature until we obtained the homogeneous solution of PLLA and glycine. Subsequently, a simple and easy spin coating process was utilized to obtain thin and flexible film of PLLA/Gly. The solution was thereafter spin coated on glass substrate at 1500 rpm for 20 s to get the desire thickness of the film. The film was then isothermally crystallized at 80 ^{o}C for 0.5 h. The thickness of the films was measured by Bruker Dektak XT-S. **Table 3.1** describes the information regarding the samples.

Table 3-1: Sample information

Sample name	**Weight percent of PLLA [wt%]**	**Weight percent of glycine as of PLLA [wt%]**	**Thickness of the film [µm]**
Neat PLLA	5	0	~17
PLLA/Gly-5		5	~18
PLLA/Gly-10		10	~15
PLLA/Gly-15		15	~24

3.2 Fabrication of PLLA/Gly thin film wearable Sensor:

The prepared films were peeled off from the glass substrate and cut into square shapes of 8 x 8 mm size. Aluminium (Al) foils were utilized as electrodes to closely sandwich both the sides (top and bottom) of PLLA/Gly film (films with dimension of ~8

mm long and ~8 mm wide). Subsequently, to isolate Al electrodes from air, polyimide tape (Kapton tape) was utilized as an encapsulation layer.

3.3 Vibration system for piezoelectricity measurement:

The PLLA/Gly film sensor (21 mm x 8 mm) was affixed to the surface of the beam (see illustration in Figure 4a (right),), and the beam was firmly fixed at one end and coupled with an electromechanical shaker (DP-V016) at the other end (**Figure 3.1**). The mechanical shaker was operated by a power amplifier with provided frequency and voltage. The voltage output was measured utilizing data acquisition system (NetdB DAQ12).

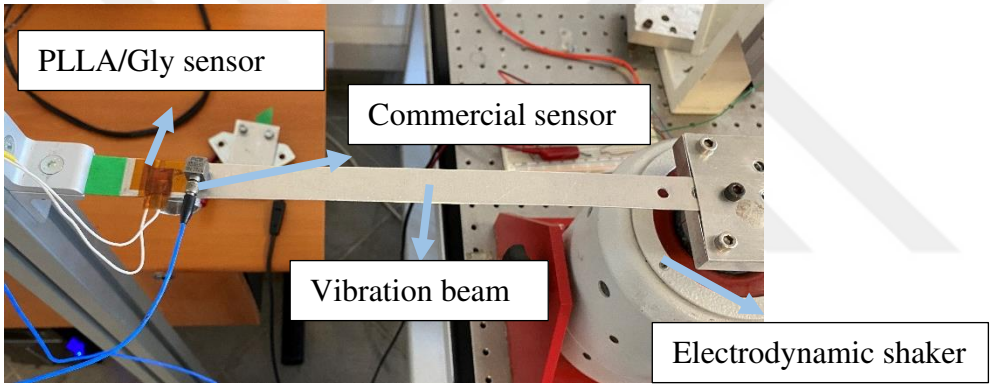

Figure 3.1**:** *Optical image of vibration testing setup*

3.4 Impact system for piezoelectricity measurement:

PLLA/Gly sensor was fixed to the rigid aluminium beam as demonstrated in **Figure 3.2** as well as in the schematic of Figure 4.7c (left). A rigid square piece of plexiglass was used to cover the sensor just to make sure that the impact force was uniformly applied to the sensor. A quartz dynamic force sensor (PCB Piezotronics (208C01), NY, USA) was used to measure force applied to PLLA/Gly sensor. The PCB sensor was installed at the bottom side of the aluminium beam at one end, that was connected to the electromechanical shaker at the other end.

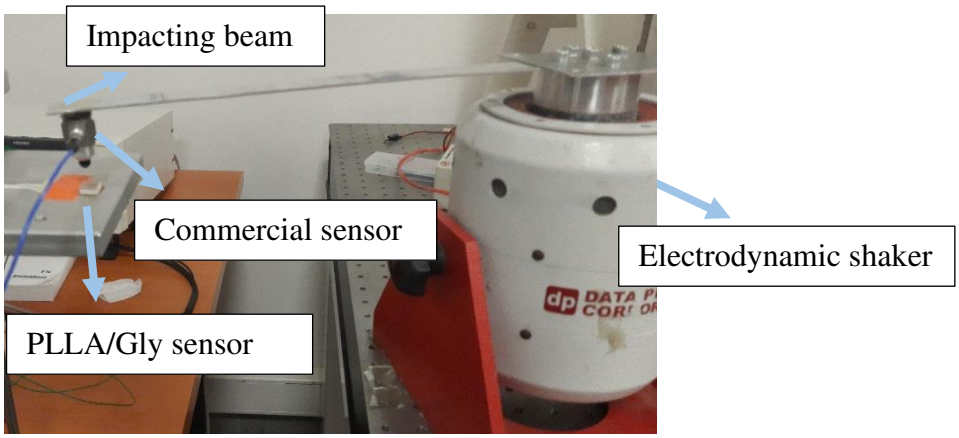

Figure 3.2*: Optical photograph of impact testing setup*

3.5 Amplification:

Stanford research systems amplifier (SR560) was used for amplification. Signals obtained from the radial and carotid artery were amplified to get better visualization of the signals. An amplification of 200 times was applied to the response obtained from radial and carotid artery pulse.

3.6 The dielectric constant calculation:

The capacitance (C) of the sample (PLLA/Gly-10) was determined first by using Impedance analyzer (MFIA Impedance Analyzer Precision LCR Meter 500 KHz- 5 MHz), thereafter, the value of εr is computed utilizing the equation ($C = \varepsilon_o \varepsilon_r \frac{A}{d}$). Vacuum dielectric constant (8.854 x 10-12 F/m) is represented by ε_o, whereas, A is representing electrode area (64 mm2), and d is the thickness of film.

3.7 Herman's Orientation Function:

The data obtained from wide angle x-ray scattering was fitted with Lorentz curve utilizing Origin Pro 2021, and the Herman's Orientation Factor was then computed from these curves. Herman's Orientation Factor (HOF) can be calculated utilizing the intensity as a function of angle (θ) around each diffraction ring. HOF (*f*) is defined in Equation 1:[183]

$$(f) = \frac{3<cos^2\theta>-1}{2} \quad (1)$$

In equation 1, $< cos^2\theta >$ is the orientation parameter and determined using the following equation:[183]

$$< cos^2\theta >_{(hkl)} = \frac{\int_0^{\frac{\pi}{2}} I(\theta) cos^2(\theta) sin(\theta) d\theta}{\int_0^{\frac{\pi}{2}} I(\theta) sin(\theta) d\theta} \quad (2)$$

Where θ is the azimuthal angle and I(θ) is the intensity scattered along the angle. By determining the HOF, it is viable to refer to the orientation of polymeric chains within the range of 0 and 1. Polymer chains are arranged in random manner if the value of HOF is near to zero, while the chains are more aligned if the value of HOF is near to 1.

3.8 Characterization of PLLA/Gly film:

***1-D XRD*:** 1-D x-ray diffraction (XRD) analysis of neat PLLA and PLLA/Gly films were conducted at room temperature utilizing a Bruker D2 phaser instrument. Size of the slit was 0.2 mm, used for Lynxeye detector. XRD patterns were recorded in the range of 5° to 45° with a step size of 0.010° and scan speed of 0.2°/min.

WAXS: Wide angle x-ray scattering measurement of PLLA/Gly films were carried out using an Anton Paar SAXSpoint 5.0 with a sample-to-detector distance of 500 mm.

***SEM*:** Scanning Electron Microscopy (SEM) were carried out on PLLA/Gly by a Zeiss Ultra Plus field emission scanning electron microscope. Square PLLA/Gly film of 6 x 6 mm was placed on the standard SEM pin (Ted Pella, Redding, CA) with carbon conductive tabs (Ted Pella, Redding, CA). 15 nm of gold (Au) was sputtered in order to overcome charging of the samples. Both SE and InLens detectors were used to obtain SEM images. Acceleration voltage of 3 kV and a working distance of 5.1 mm were set for the measurements.

3.9 Differential scanning calorimetry:

Differential scanning calorimetry (DSC) analysis was conducted for neat PLLA and PLLA/Gly composite films utilizing a DSC, (NETZSCH STA 449 F3 Jupiter). Approximately, 3 mg of each specimen was loaded into an aluminium pan with lid and

pressed to seal the pan. An empty pan of aluminium was considered as reference, and sample heated from 0 ºC to 210 ºC at the rate of 10 ºC/min. And to make sure the sample is completely melted; the sample was held for 5 minutes at 210 ºC (first cycle). The second cycle was completed by cooling the sample from 210 ºC to 0 ºC at the rate of 10ºC/min. The sample was again heated from 0 ºC to 210 ºC at the rate of 10 ºC/min to complete the third cycle.

3.10 Fourier transform infrared spectroscopy:

Fourier Transform Infrared (FTIR) spectra were recorded using Nicolet™ iS™ 10 FTIR Spectrometer with a range of spectrograms from 800 to 4000 cm^{-1}.

3.11 Current and power density measurmen:

The following relation, $P = \frac{V^2}{A \cdot R_L}$ was used to compute the output power density. Where, V is the voltage drop across R_L, and A is the effective area of the sensor.

Chapter 4:

RESULTS AND DISCUSSION

Disclaimer: This chapter (4) is adapted from the following article with permissions of all co-authors and journal:

Ali, Mohsin, et al. "A Flexible and Biodegradable Piezoelectric-Based Wearable Sensor for Non-Invasive Monitoring of Dynamic Human Motions and Physiological Signals." Advanced Materials Technologies: 2300347.

My contribution: conceptualization, design, fabrication, experiments, figures, and writing.

This chapter describe the results and discussion of this study in detail.

4.1 Fabrication of wearable piezoelectric sensor

Figure 4.1 illustrates the fabrication process of the flexible piezoelectric film and wearable pressure sensor, the biodegradability of piezoelectric PLLA/Gly film, and real-time applications of the fabricated sensor. The development of biodegradable piezoelectric material and the fabrication of flexible sensors are as follows: first, a PLLA solution mixed with different weight percentages of Gly was prepared, and the solution was spin coated to get the piezoelectric thin films (**Figure 4.1**a). Subsequently, PLLA/Gly film was annealed at 80 ^{o}C for 30 min, followed by peeling it off from the glass slide. Then, to enhance the performance of piezoelectric biodegradable PLLA/Gly film, the content of glycine in PLLA was optimized (see **Table 1.1, materials and methods)** followed by choosing the optimal piezo film for further device demonstrations. Finally, the prepared piezoelectric PLLA/Gly film was sandwiched between two aluminum electrodes (top and bottom), and Kapton tape was used to encapsulate the sensor in order to minimize any errors in data measurement due to triboelectric effects (**Figure 4.1**b). The PLLA polymer and Gly combined as a result of hydrogen bonding between PLLA and Gly molecules, disintegrate in phosphate-buffered saline (PBS) solution as can be seen from reaction scheme (**Figure 4.1**c). The prepared piezoelectric PLLA/Gly film gradually degraded in PBS solution within five days at 37 ^{o}C (**Figure 4.1**d). The fabricated sensor was demonstrated as a wearable device for the detection of human pulse rate (carotid and radial artery) and other critical physiological signals such as wrist and elbow movement (bend and release) and swallowing and coughing actions (**Figure 4.1**e).

In previous reports, amino acids have been used as heterogeneous nucleating agents to increase the crystallization rate and the degree of crystallinity of several polymers like PLA.[79–85] In this way, the amount of Gly as a nucleating agent is optimized to increase the degree of crystallinity of PLLA. In addition, they do not affect the biodegradability of PLA. Glycine is a type of amino acid, and it has extensively been used in drug administration.[190] Glycine comprises a backbone structure like PLLA with an acidic COOH group and a primary NH_2 group, but with different side chains. Maria et al. utilized glycine amino acid as a heterogeneous nucleating agent to analyze the impact of the isothermal crystallization behavior of PLA. They found that glycine possesses a substantial nucleating ability (54.1%).[191] Incorporating glycine as a nucleating agent is

preferred since PLLA and glycine are comprised of similar chemical structures enabling crystal formation.

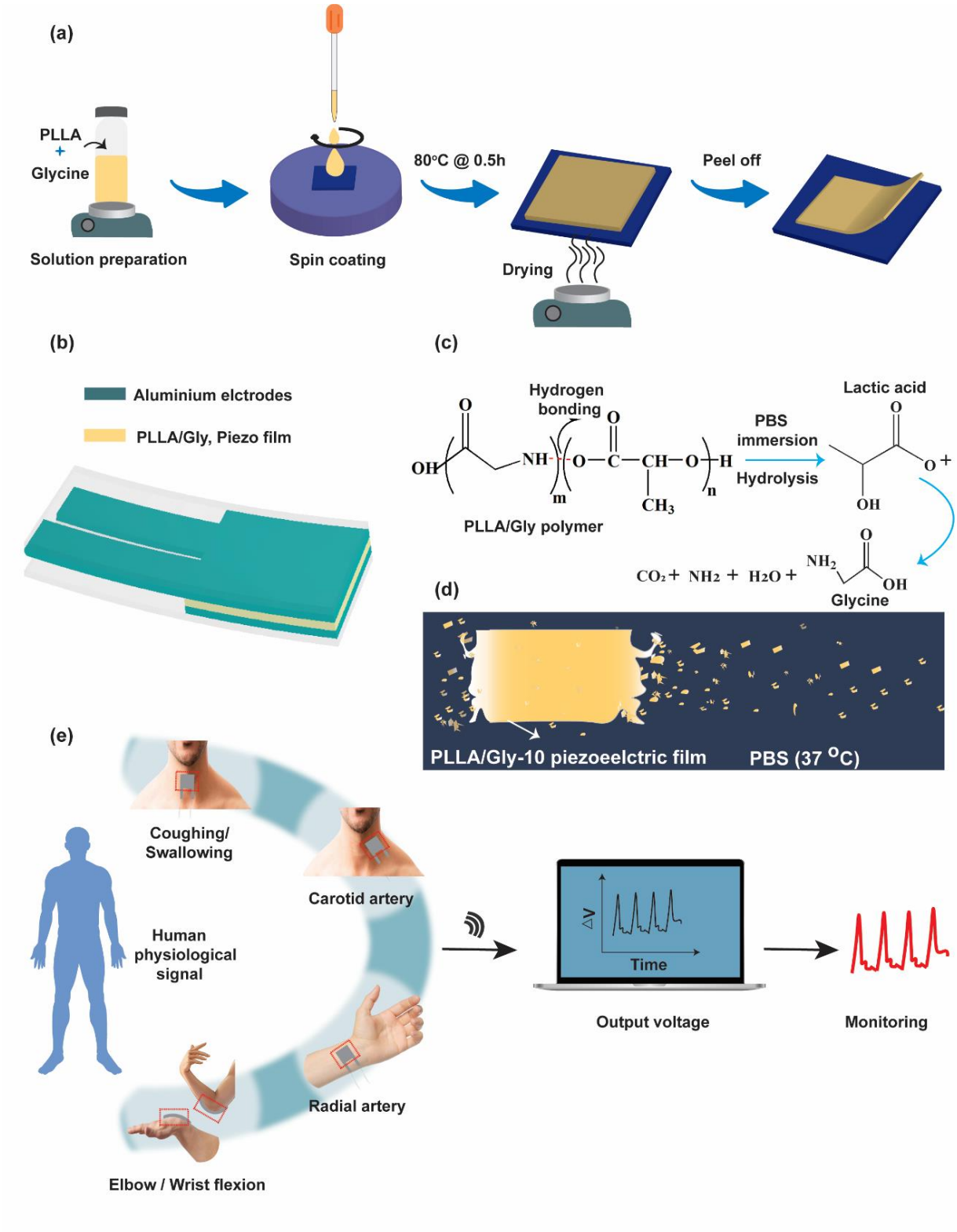

Figure 4-1*: a) Schematic demonstration of the fabrication process for biodegradable piezoelectric PLLA/Gly film. A solution of PLLA/Gly spin-coated to get the desired thickness of the film (~15 µm), followed by drying at 80 °C for 30 min and peeling off from the glass slide. b) Schematic illustration of self-powered wearable sensor based on biodegradable piezoelectric film sandwiched between two aluminum electrodes and then encapsulated by polyimide tape (Kapton) to compactly sandwich the piezo film/Al assembly. c) Disintegration of PLlA/Gly polymer due to hydrolysis when immersed in PBS solution. d) Schematic illustration of PLLA/Gly piezoelectric film degradation in PBS solution at 37 °C for five days. e) Schematic demonstration of the real-time applications of the flexible piezoelectric sensor in healthcare monitoring. Images of the body parts, along with a laptop, are created with freepik.com.*

4.2 Structural and morphological analysis

The degree of crystallinity and orientation are two main properties of PLLA polymer that should be improved to induce piezoelectricity in PLLA.[64,71] The piezoelectricity generated in PLLA under impact is due to the net polarization occurring due to the relative alignment of the C=O bond growing out from the PLLA backbone. To induce net polarization in PLLA, the molecular chains are required to be aligned in a similar direction forming an organized crystalline domain. In previous reports, researchers have used electrospun fibers of PLLA and a thermally drawn and compression-molded PLLA to develop flexible piezoelectric films. [178,181,185,192] However, there were some major constraints, such as instability of the electrical signals generated from electro-spun membranes of PLLA under an applied force.[181] Additionally, output signals are often mixed with the signals produced by the triboelectric effect (electric signals produced by the friction between electrodes and film).[192]

Therefore, in this work, to obtain piezoelectric PLLA film without stretching or electrospinning PLLA, glycine (amino acid) is utilized to increase the degree of crystallinity of PLLA. X-ray diffraction (XRD) and differential scanning calorimetry (DSC) analysis was performed to study the crystallization behavior of PLLA and PLLA/Gly films. **Figure 4.2**a demonstrates the XRD patterns of neat PLLA and

PLLA/Gly films. Neat PLLA (without glycine) shows three broader peaks (amorphous nature) at 15°, 17°, and 19°, referring to the [010], [110]/[200], and [203] orientations of α-crystals, respectively.

Following the addition of glycine, PLLA exhibits three crystalline orientations [111], [200], and [110], and glycine crystal peaks are observed at 29.9° and 35.6°. With the addition of glycine content (i.e. 5, 10 and 15 wt% as of dry PLLA) in PLLA, the maximum intensity and sharpness of [200] and [110] peak were observed in the case of 10 wt% glycine content. This attributes to the transformation of α- form crystal structure having a left-handed 10_3 spiral shape to the β-form crystal formation having 3_1 spiral shape.[193] In other words, the growing crystal structures are aligned or oriented more in [110] and [200] directions, turning it into piezoelectric PLLA (β-form). The increase in the intensity and sharpness of the glycine peak at 29.9° was also observed for the PLLA/Gly-10 sample. The XRD peak at 29.9° indicates the formation of the α-glycine phase, which is the thermodynamically more stable phase of the glycine.[99] Glycine has three polymorphic phases (α, β, and γ) under ambient conditions. α-Glycine is known to have non-piezoelectric properties because of the centrosymmetric structure without piezoelectricity, while β-glycine and γ-glycine contain piezoelectric features owing to the non-centrosymmetric polar structure. Thus, the primary source of piezoelectricity is from treated PLLA (β-form). Utilizing XRD data, the degree of crystallinity of PLLA was also computed based on the ratio of area under the [200] and [110] peaks to the area under the whole curve (**Figure 4.3**). When the amount of glycine was increased to 15% by weight in PLLA, the intensity and sharpness of the peaks decreased, which might be due to the formation of glycine agglomerates. 2D-XRD analysis was conducted to estimate the orientation of crystalline structures after the addition of glycine. Likewise, a specific amount of glycine in PLLA enhances the degree of orientation of crystal domains, as shown in the two-dimensional XRD image in **Figure 4.2**b. 2D-XRD photographs display the orientation of crystal domains inside PLLA, crystallized with glycine. The amorphous circle changes to a band as the film contains more aligned crystals. The less the sign band diverges from the axis, the more aligned the crystals film will have.[22,185] As can be seen from the sample with 10 wt% glycine, less signal band diverges from the axis, which means it has a more aligned structure than other combinations. Herman's Orientation Function (f) commonly expresses the orientation degree, which symbolizes the average alignment of the pole relative to some reference orientation.[194] With the addition of 10

wt% glycine in PLLA, the dispersion angle decreases while Herman's Orientation Function increases **(see material and methods)**. The degree of orientation for PLLA/Gly-5, PLLA/Gly-10 and PLLA/Gly-15 samples was computed around ~0.69, ~0.51, and ~0.54, respectively. Thus, the PLLA/Gly-10 composite film has high crystallinity than other samples and the results presented in **Figure 4.2a** agree with 2D

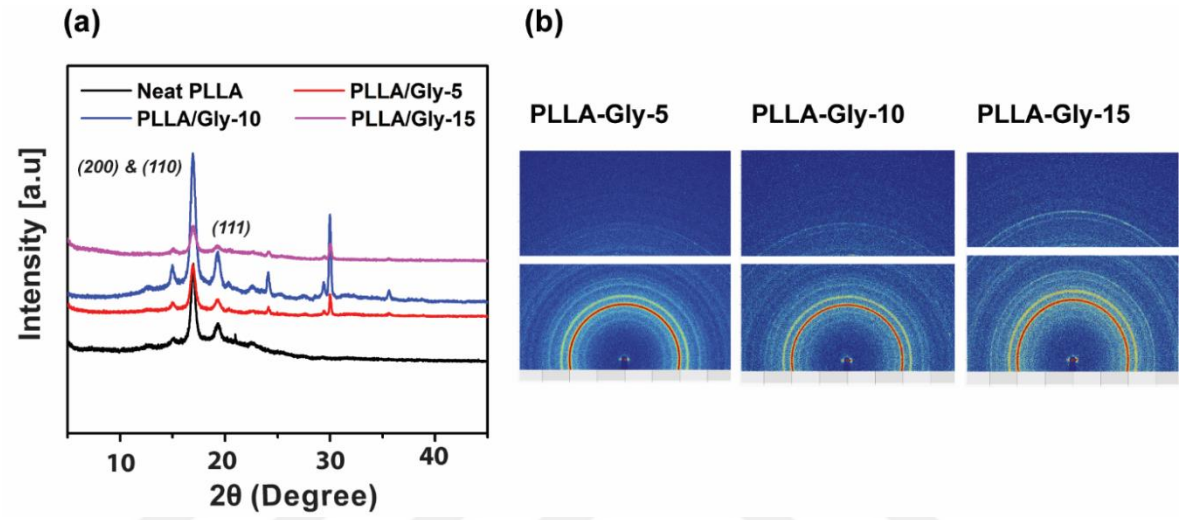

Figure 4.2**:** ***Characterization of crystallinity and polymer chain orientation for PLLA/Gly films.*** *a) One-dimensional (1D) XRD results for PLLA/Gly films with different weight% of glycine. b) Two-dimensional XRD photographs depict the orientation of the polymer chain of PLLA films with different glycine content.*

XRD data (**Figure 4.2**b). These results describe an optimal weight percent of glycine (10 wt%) to obtain a flexible piezoelectric PLLA/Gly-10 film with improved crystallinity and promising piezoelectric effect.

Furthermore, the crystallinity of α-crystals decreases, and the crystallinity of β-crystals increases, which could be due to the interaction between amine bonds in glycine and ester groups in PLLA. This subsequently improves the orientation of PLLA chains, ultimately increasing the crystallinity of β-form.[195] Thus, the main source of piezoelectricity in PLLA/Gly composite film is from PLLA.

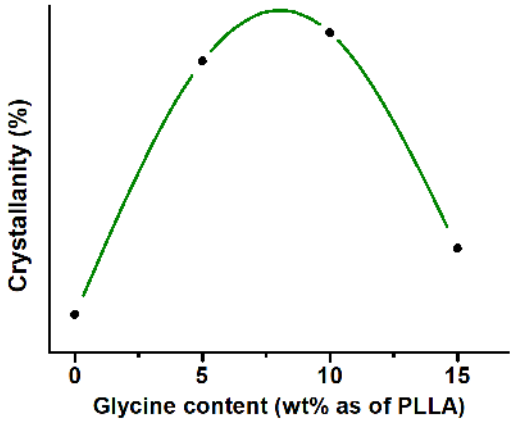

Figure 4-3*: Percent degree of crystallinity of PLLA/Gly films as a function of glycine content.*

Figure 4.4 illustrates differential scanning calorimetry curves for pure PLLA and PLLA/Gly samples with different weight percent of glycine. DSC thermograms demonstrate that all the samples provide similar thermal transition peaks. The melting peak of neat PLLA appeared at ~175 ^{o}C, while the melting peak of PLLA/Gly films noticed in the range of 160-170 ^{o}C and these peaks are partially overlapped, corresponding to α and β-crystals of PLLA.[196] Further, with the incorporation of glycine, the melting enthalpy of the β-crystals increases, ascribing to the increase in crystallinity of the β-form PLLA improved. This improvement in crystallinity was observed for samples containing a certain amount of glycine i.e., 5 and 10 wt% glycine. With further increase in glycine (i.e., for 15 wt%) the crystallinity of the PLLA/Gly film starts decreasing, which may be due to decrease in interaction between PLLA and glycine.

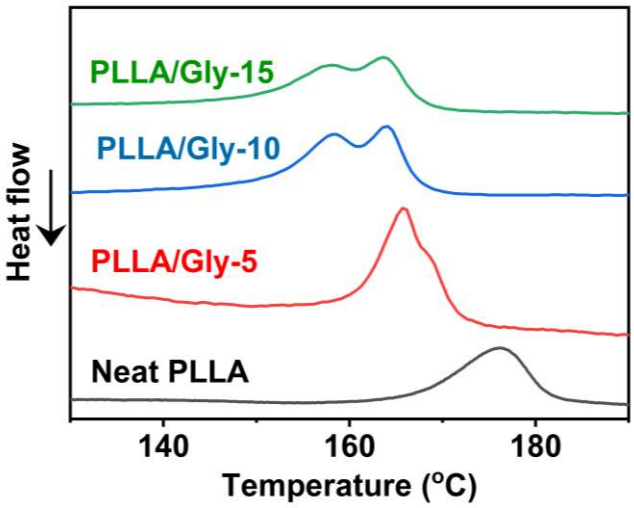

Figure 4-4*: DSC thermograms of neat PLLA and PLLA/Gly films*

We have analyzed FTIR spectroscopy of neat PLLA and composite samples to probe the interaction between PLLA and glycine. **Figure 4.5** shows the FTIR spectra of neat PLLA and PLLA/Gly composite samples. The peak appeared at 1747 cm^{-1} attributes to the vibration of ester bond present in PLLA (**Figure 4.5**b). Addtition of glycine content (5 wt% and 10wt%), results in shifting the ester bond of PLLA to the lower frequency regions because of the interaction between amino and caboxyl groups of glycine and ester group of PLLA (**Figure 4.5**b). Whereas, for the sample containing 15 wt% glycine, a slight shifting of C=O is observed, which is likey due to the less intermolecular interaction between PLLA and glycine. Ranging from 3200 to 3600 cm^{-1}, a broader hydrogen-bond peak is noticed, corresponding to the hydrogen bonds among the molecular chains of PLLA and those between amine bond of glycine and C=O group of PLLA are formed (**Figure 4.5a**). The interaction between PLLA and glycine and the formation of a hydrogen bond (**Figure 4.5**c) improves the chain alignment of the samples, possibly enhancing the piezoelectric properties of the PLLA/Gly composite.

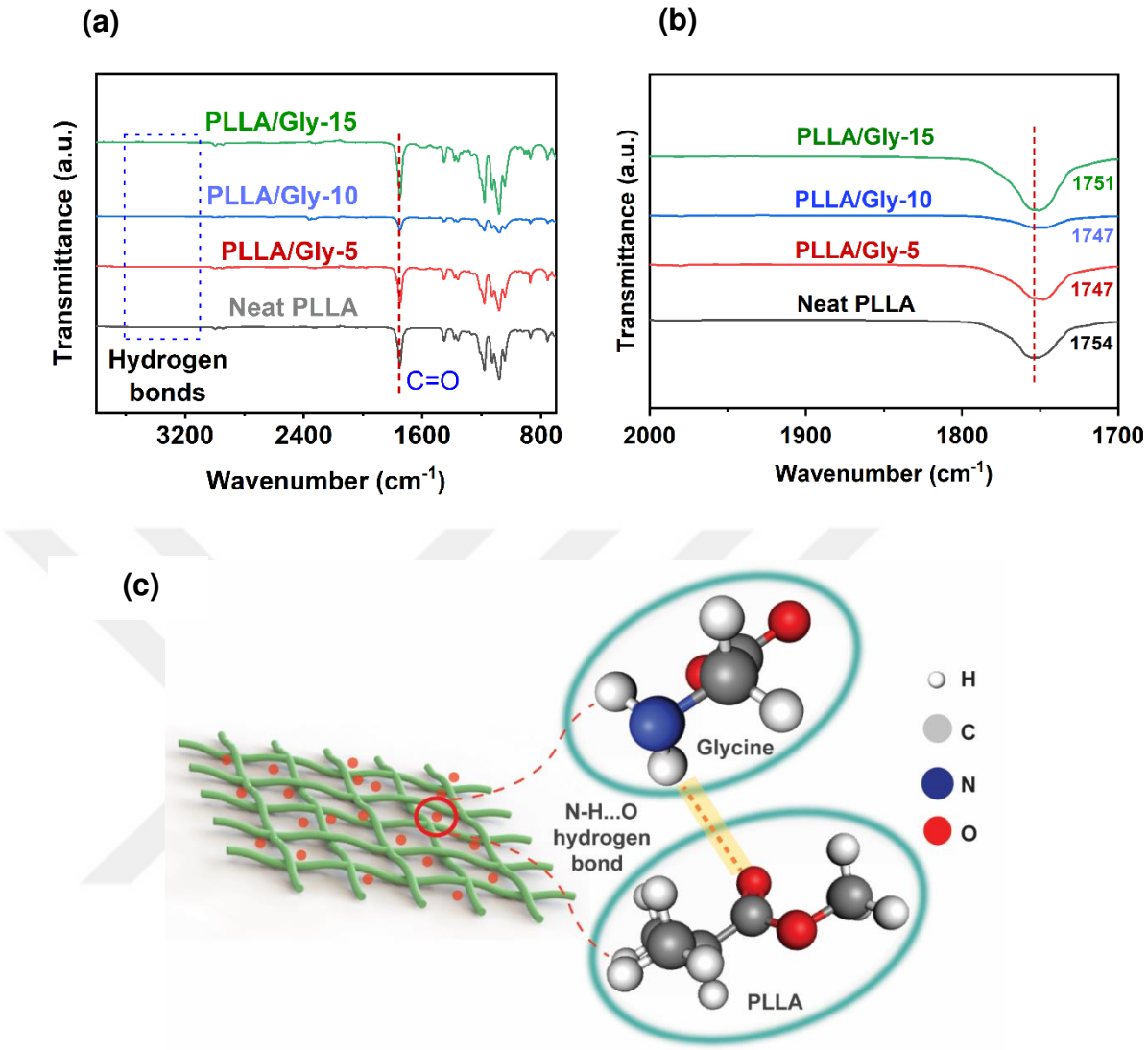

Figure 4-5**:** *(a-b) FTIR spectra of neat PLLA and PLLA/Gly films in the range of 800-4000 cm^{-1}. (c) Schematic illustration of intermolecular hydrogen between PLLA and glycine molecules.*

PLLA is a semicrystalline polymer containing a significant part of an amorphous network but also comprises several crystal nuclei that rapidly grow with the addition of nucleating agents.[197] The amorphous network of PLLA polymer is highly isotropic and retains a center of symmetry. In order to change the isotropic nature of polymer chains to be piezoelectric, the center of symmetry must be eliminated.[198] The addition of a very small amount of nucleating agent improves the crystallinity, accelerates the crystallization, triggers a particular crystalline structure and morphology etc.[199,200] Utilizing glycine content as nucleating agent results in introducing highly oriented new crystal structures. **Figure 4.6**a-c illustrates an SEM examination of the PLLA film surface

with 10 wt% glycine content that displays the morphology of PLLA/Gly-10 composite film. The addition of 10 wt% glycine largely enhances the nucleation of PLLA by creating more nucleating sites, thus improving its crystallinity. The highly oriented crystal structures with the linear interface between them show that these structures nucleated simultaneously (Figure **4.6**a and **4.6**b). Numerous crystalline regions grown within the amorphous regions exhibit an organized orientation (Figure **4.6**c). Likewise, an aligned network of polymer chains is anisotropic, an organized distribution of crystallites is also anisotropic. The intruding crystal structures having a nucleus in the center, and spread out dendritically from the nucleus, as depicted in Figure **4.6**d.[201] The orderly distribution of crystallite structure comprises crystal lamellae connected by amorphous regions of PLLA (Figure **4.6**c and **4.6**d).

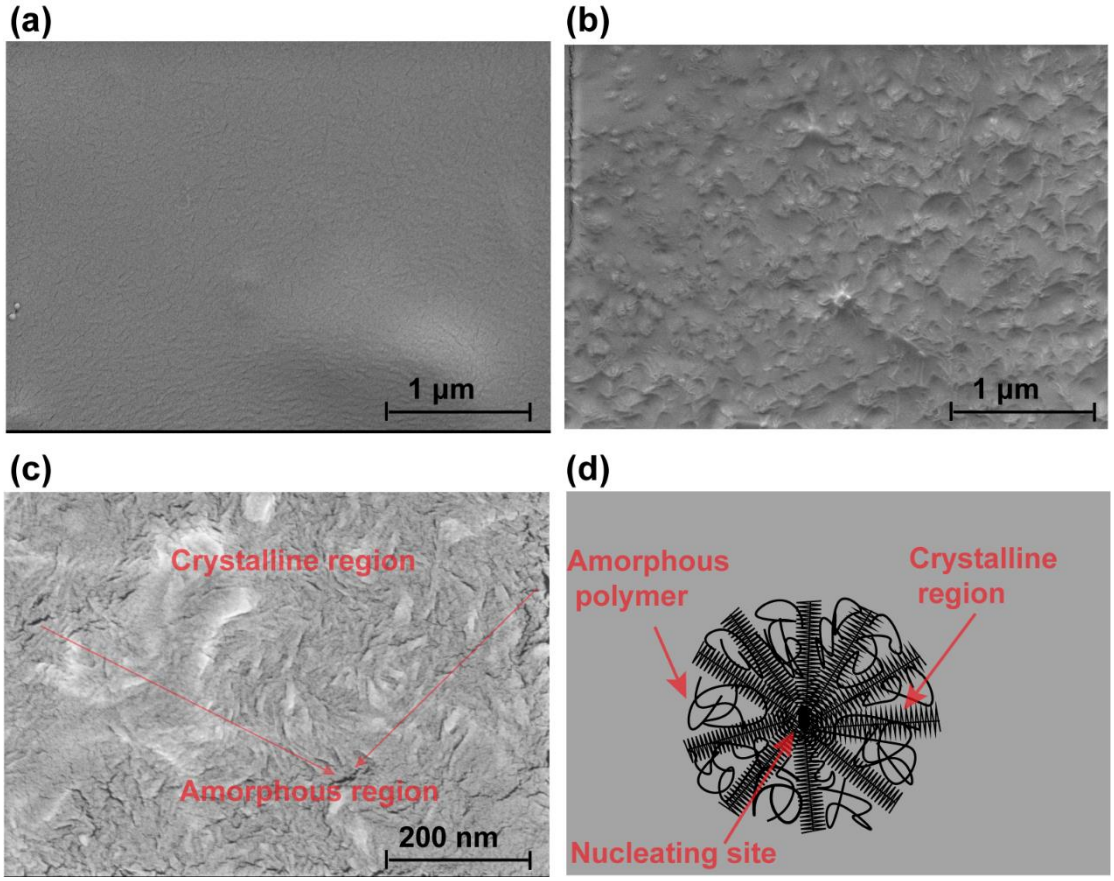

Figure 4-6**:** *a-c) SEM images of crystallized PLLA/Gly-10 film at ambient conditions. d) Schematic illustration of crystalline structure comprises crystal lamellae connected by amorphous regions.*

4.3 Piezoelectric characterization

Vibration and impact tests were conducted to assess the piezoelectric voltage outputs of the PLLA/Gly films under mechanical forces/strains, which have also been utilized for characterizing other piezoelectric materials.[202,203]

The PLLA/Gly film was sandwiched between two aluminum electrodes and encapsulated in Kapton tape for vibration testing. The sensor was firmly affixed to the top portion of the aluminum beam with Kapton tape. Due to the triboelectric effects, Kapton tape was used to avoid errors in output signals. During the measurements, it was assured that the signals were not generated by triboelectricity or wire motion. The beam is fixed from one end, and the other side is attached to the electrodynamic shaker that controls the desired frequency and force levels (SI). The sensor is exposed to mechanical strains (**Figure 4.7**a, inset) by generating controlled oscillations using the setup. The impact testing system included a commercial force sensor (PCB) to measure the impact level, and the same electrodynamic shaker to produce dynamic forces on the PLLA/Gly-10 sensor (**Figure 4.7**c (left), inset). In both testing procedures, the sensor's output voltage is measured by a data acquisition system (NetdB DAQ12). **Figure 4.7**a shows open-circuit voltage outputs from PLLA films with different weight percent of glycine when it is subjected to vibration force at 41 Hz. Although the PLLA films with different percentage of glycine responded to the input with different piezoelectric response.

The neat PLLA film (control sample) produced only noise. The results show that the sample with 10 wt% of glycine in PLLA has the maximum signal output, showing the optimal amount of glycine. For the remaining measurements, the experiments were conducted only with piezo PLLA/Gly-10 film (10 wt% glycine as of dry PLLA) since significant piezoelectricity was acquired with this sample. In addition, this film is uniform and highly flexible. Thus, for further characterization of the sensor, PLLA/Gly-10 was chosen as the optimal piezoelectric film. **Figure 4.7**b depicts that sensor fabricated from neat PLLA and PLLA/Gly-10 film were subjected to the same force level (~4.5 N). **Figure 4.7**c (left) shows the open-circuit voltage output from the sensor fabricated with the optimal piezo film (PLLA/Gly-10) and neat PLLA. An input force of ~4.5 N was applied to a sensor made by using optimal piezo film that resulted in a generation of peak-to-peak voltage output of ~0.42 V, while the sensor made of neat PLLA resulted in only noise.

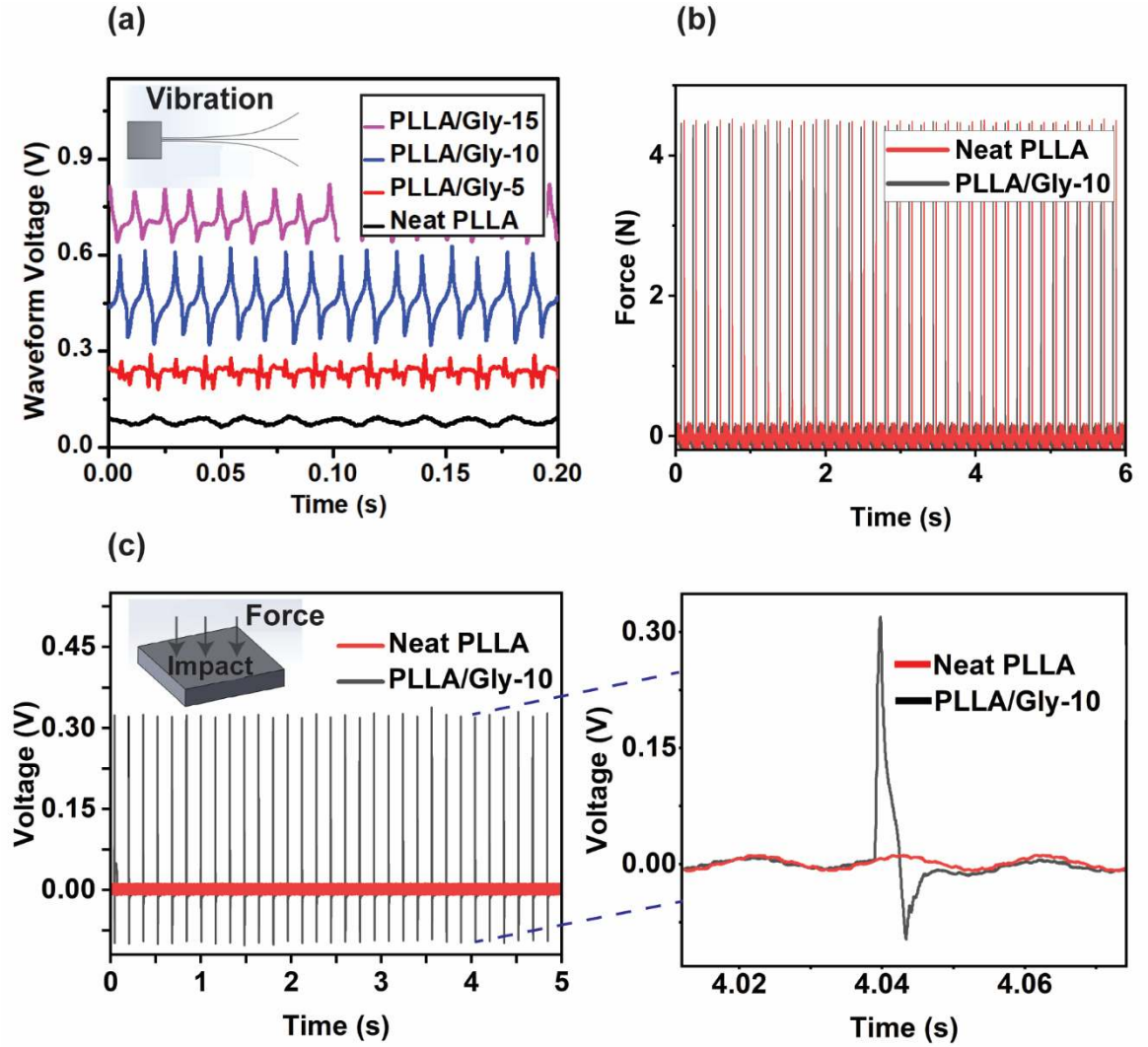

Figure 4-7**:** *Measurement of piezoelectric PLLA/Gly output voltage from vibration and impact modes. a) Output voltage from neat PLLA and PLLA/Gly with different glycine content under vibration at 41 Hz. Simplified illustration of vibration setup used to get the output voltage (Inset) b) Same impact force applied to neat PLLA and PLLA/Gly-10. c) Output voltage from neat PLLA and PLLA/Gly-10 (left) subjected to the same force. Simplified schematic demonstration of impact setup (Inset of figure 4c (left)). (Right) enlarged view of output voltage.*

The voltage output increased linearly with increasing applied force (**Figure 4.8**). Hence, the piezoelectric output of the sensor increased almost linearly from ~0.03 V to ~0.42 V under applied pressure ranging from 3.2 to 69.5 kPa (**Figure 4.8**).

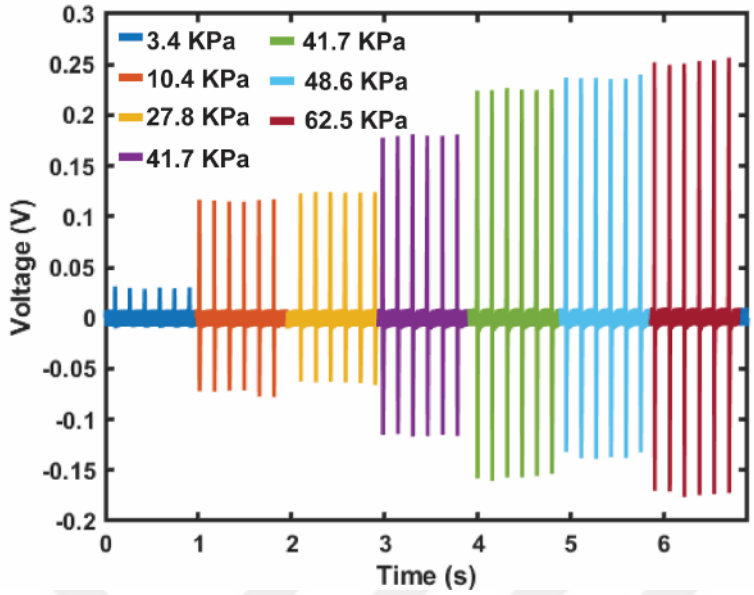

Figure 4-8**:** *Voltage output generated by piezoelectric pressure sensor under different dynamic impact loading (force).*

The sensitivity, response time, and durability of the piezoelectric pressure sensor were characterized to validate the applicability of the sensor in detecting vital signals. Different known pressures/forces were applied, ranging from 3.2 to 69.5 kPa, on the piezoelectric sensor to calibrate output voltage. The distinct and clear output signals at different pressures permitted us to construct a calibration curve (**Figure 4.9**a). The calibration curve could be useful for measuring pressures ranging from 0 to 69 kPa. Biodegradable piezoelectric PLLA/Gly-10 film could also be assembled with other metal electrodes such as silver, nickel and gold for bio-compatible wearable applications. Moreover, biodegradable electrodes such as magnesium and molybdenum can also be used to fabricate a completely biodegradable piezoelectric sensor based on PLLA/Gly-10 film. Therefore, it could be utilized to measure physiological pressures such as intraocular pressure (0-5.3 kPa)[204] and monitor diaphragmatic contraction.[22]

The correlation between input pressure and voltage output can be described by two linear regions. Up to the 10 kPa pressure range, the slope obtained from the linear fit of voltage output is 0.02245 $V.kPa^{-1}$, e.g., the sensitivity of 0.02245 $V.kP^{-1}$. When the magnitude of pressure increases above 10 kPa, a slope of 0.004 V kPa^{-1} is obtained from the linear fit of the voltage output, e.g., a sensitivity of 0.004 V kP^{-1}. The non-linear

deformation of the PLLA/Gly-10 film as a function of input pressure may display two sensitivities.

The response time refers to an increase in output voltage from the base point to the maximum point in response to the force applied to the sensor, which was assessed to be ~10 ms upon pressure application. Whereas descent time is the recovery phase where output voltage reaches the base point when force is removed, which was calculated around ~26 ms in our case. The recovery time (~26 ms) (descent phase of peak) is slightly longer than the response time (ascent phase of peak), possibly because the device needs more time to recover from its shape change. **Figure 4.9**b depicts the response time of PLLA/Gly-10, e.g., 10 ms, which is even faster than other pressure sensors (31-410 ms).[205–207] This could be attributed to the high orientation of polymer chains and chemical stability of β-form of PLLA.

The accuracy of our sensor's signals is compared with a piezoelectric quartz force sensor (a commercially available PCB piezotronics; 208C01). Utilizing the calibration curve plotted for our sensor, output voltage transformed to a force value. As shown in **Figure 4.9**c, the obtained signals closely correspond to the magnitude of applied force measured by the commercial sensor. Further, the sensor's long-term stability (mechanical durability) was assessed by applying dynamic pressure (31.25 kPa) over 4000 cycles at a 5 Hz frequency, as illustrated in **Figure 4.9d**. The voltage output response was relatively stable and displays no major instability during periodic loading (see inset of **Figure 4.9**d).

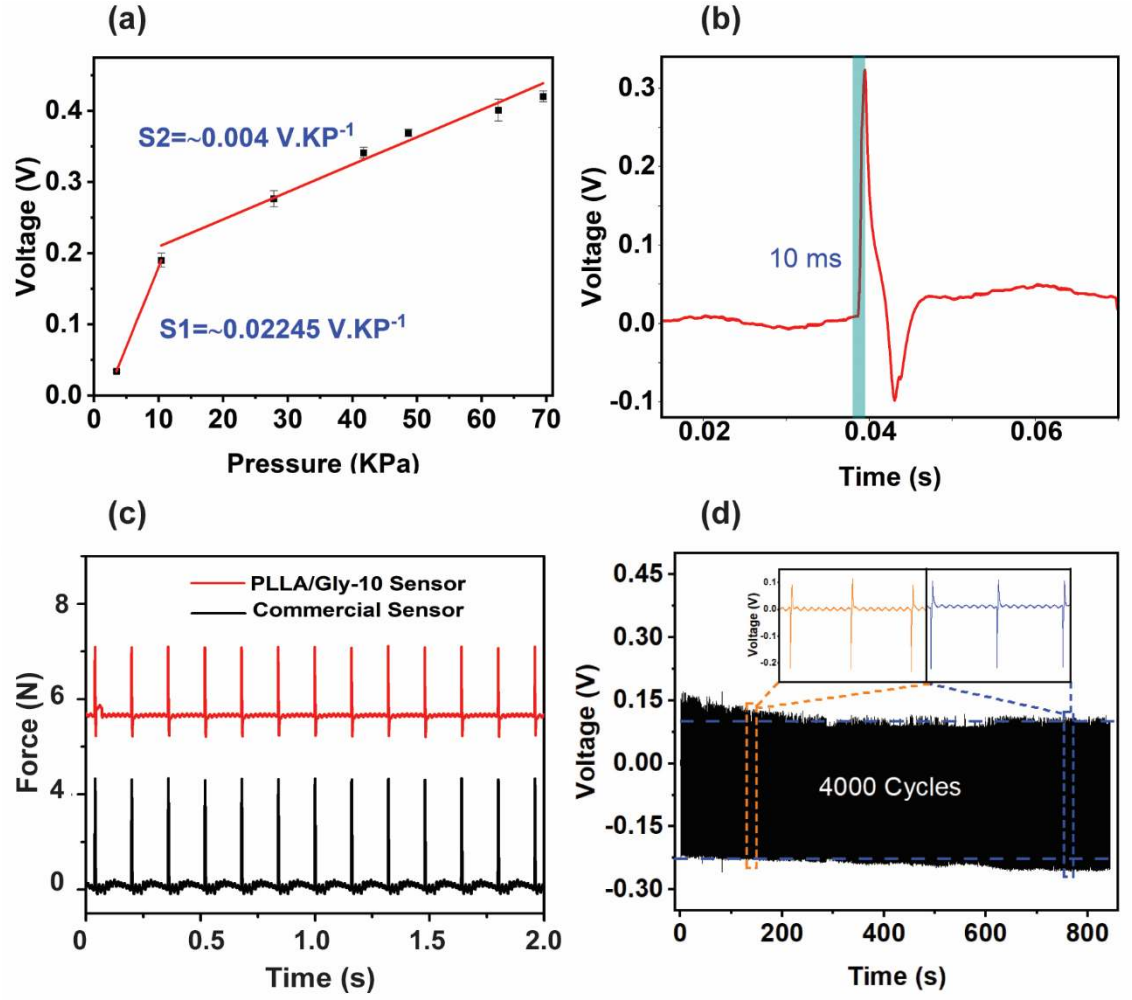

Figure 4-9**:** *a) A typical calibration curve generated from PLLA/Gly-10 sensor under different input pressures. The piezoelectric sensor displays good linearity and sensitivity ranging from 3.2 to 69.5 kPa. b) Response time of PLLA/Gly-10. c) Output signals from commercial (PCB piezotronics sensor) and PLLA/Gly-10 sensor. d) Long-term (mechanical) durability test of the piezoelectric sensor under dynamic loading conditions with impact pressure of (31.25 kPa) and frequency of 5 Hz. The inset demonstrates an enlarged view of voltage output versus time.*

In this study, we focused on developing a biodegradable material based piezoelectric sensor. We have compared the developed sensor with already existing sensors and presented them in **Table 4.1**. The developed bioresorbable piezoelectric film exhibits good sensitivity, response time, and considerable durability (**Figure 4.9**), which is better than most of the sensing devices mentioned in Table 2. Moreover, the bioresorbable

piezoelectric film possesses high sensitivity (13.2 mV kPa^{-1}) when compared to other bioresorbable piezoelectric materials.

Table 4-1: Comparison of performance of different mechanical sensors

Mechanism	Materials	Sensitivity	Ref
Piezoresistance	Lead titanate (PbTiO3) nanowires/ graphene	9.4 × 10−3 kPa^{-1}	[208]
	Graphene/paper	0.26 kPa^{-1}	[209]
	Polydimethylsiloxane (PDMS)/carbon nanotube	0.34 kPa^{-1}	[210]
Triboelectricity	Au nanowires/carbon nanotubes/PDMS	5.2 mV kPa^{-1}	[211]
Piezoelectricity and triboelectricity	PEDOT:PSS/PTFE/ PZT	5.7 mV kPa^{-1}	[212]
Piezoelectricity	PVDF-ZnO	0.33 V kPa^{-1}	[213]
	Nylone-11	0.13 mV kPa^{-1}	[214]
	Polyacrylonitrile (PAN)/PVDF	-	[205]
	Collagen	27 mV N^{-1}	[163]
	Chitosan/β-glycine	2.82 ± 0.2 mV kPa^{-1}	[99]
	Lithium niobate	28.8 nA kPa^{-1}	[215]
	Imidazolium perchlorate (ImClO4)/ bacterial cellulose (BC)	4.24 mV kPa^{-1}	[15]

	PLLA/Gly	13.2 mV kPa^{-1}	This work

4.3.1 D_{33} coefficient measurement

We computed the longitudinal piezoelectric charge coefficient d_{33} (expressed in pC N^{-1}) utilizing the following relation.[216]

$$d_{33} = \frac{\varepsilon_o \varepsilon_r}{d} \left(\frac{\Delta V}{\Delta P}\right) \quad (1)$$

Where the thickness of the film, dielectric constant, and vacuum dielectric constant are represented as d, ε_r and ε_o(8.854 x 10^{-12} $F.m^{-1}$) respectively. The sensitivity of the sensor is shown by $\Delta V/\Delta P$. The calculation of the dielectric constant is explained in method section of the supporting information. In this case, the value of ε_r was found to be 0.6192 at room temperature. Utilising these values, the longitudinal piezoelectric charge coefficient, d_{33}, is estimated as ~8 pC/N, which is in the range of previous reports.[67]

4.4 Real-time monitoring of human physiological signals

Direct monitoring of physiological signals, including arterial pulse (radial and carotid) and muscle movement utilizing a piezoelectric sensor, has great potential in identifying human health information. **Figure 4.10**a displays a photograph of a piezoelectric sensor conformally affixed to the human wrist with a transparent adhesive thin film (3M Tegaderm) for detecting radial pulse rate. Stable deformation of the device results in effectively responding to the movement of blood vessels due to the good flexibility of the sensor, as depicted in the inset of **Figure 4.10**a. A healthy male under thirty with no skin wounds, no allergic reactions, or ailments was considered for demonstrations. Approximately 72 beats per minute (BPM) and an average voltage (V_{pp}) of 700 mV (with amplification, see materials and method section) were generated by radial artery pulse. Important physiological and biomedical information, including blood pressure and arterial stiffness, can be inferred from the characteristic peaks of peripheral artery waveforms exhibited by an enlarged view of the pulse signal (inset of **Figure**

4.10b). In the normal state, peaks P_1 and P_2 indicate the sum of traveling and reflected waves (from the hand) and waves reflecting from the lower body deducted by the end-diastolic pressure, respectively. The difference in time of peaks P_1 and P_2 is denoted as ΔT_{DVP}, and the ratio of P_2 to P_1 is termed as radial artery augmentation index (AI_r), which strongly correlates with arterial stiffness.[217] The average values measured for ΔT_{DVP} and AI_r were 0.15 and 1.05 s, respectively, which are compatible and correspond to a person under thirty, as stated by Nichols.[218] We then conformally attached the piezoelectric sensor to the human neck for non-invasive monitoring of other human physiological activities such as carotid artery pulse (**Figure 4.10**c). The voltage output (V_{pp}) generated from the carotid artery pulse (top panel, with amplification) was 400 mV, as demonstrated in **Figure 4.10**d. Using MATLAB, we applied low and bandpass filters to refine the data obtained for radial and carotid artery pulse using an oscilloscope (Rohde & Schwarz RTE 1034). More than 50 Hz of noise produced from the surrounding environments was refined using a low and band pass filter.

The device was then attached around the throat to detect the movement of muscles while coughing and drinking (**Figure 4.10**e). The piezoelectric sensor shows high sensitivity to the movement of the esophagus muscle (the food pipe), allowing it to detect signals produced by the esophagus during the vibration of the vocal cord (coughing) (**Figure 4.10**f). It could effectively detect the glottis' opening and closing physiological features during swallowing (**Figure 4.10e**).[219] Thus, the wearable sensor could be useful in examining breath for the early detection of sudden infant death syndrome (SIDS).[220] Moreover, the sensor also showed high accuracy in detecting vocal cord vibration during the repetitive action of coughing. Thus, the wearable sensor can also be used to examine a patient's chronic obstructive pulmonary disease (COPD) and damaged vocal cords, including chronic bronchitis, asthma, etc., by evaluating the output signals of coughing action.[219]

In addition, we attached the wearable piezoelectric sensor to the human wrist and elbow (**Figure 4.10**g and **4.10**i). Bending and releasing actions of both the wrist and the elbow led to the generation of clear voltage output signals due to the shear deformation of the piezoelectric film. Repetitive bending of the wrist and elbow produces a piezoelectric potential within the device, which generates a positive peak. A peak with negative amplitude appears upon release due to the reverse piezo potential (**Figure 4.10**h

and **4.10**j). This demonstration shows the tactile sensing capabilities of the wearable sensor during human activities.

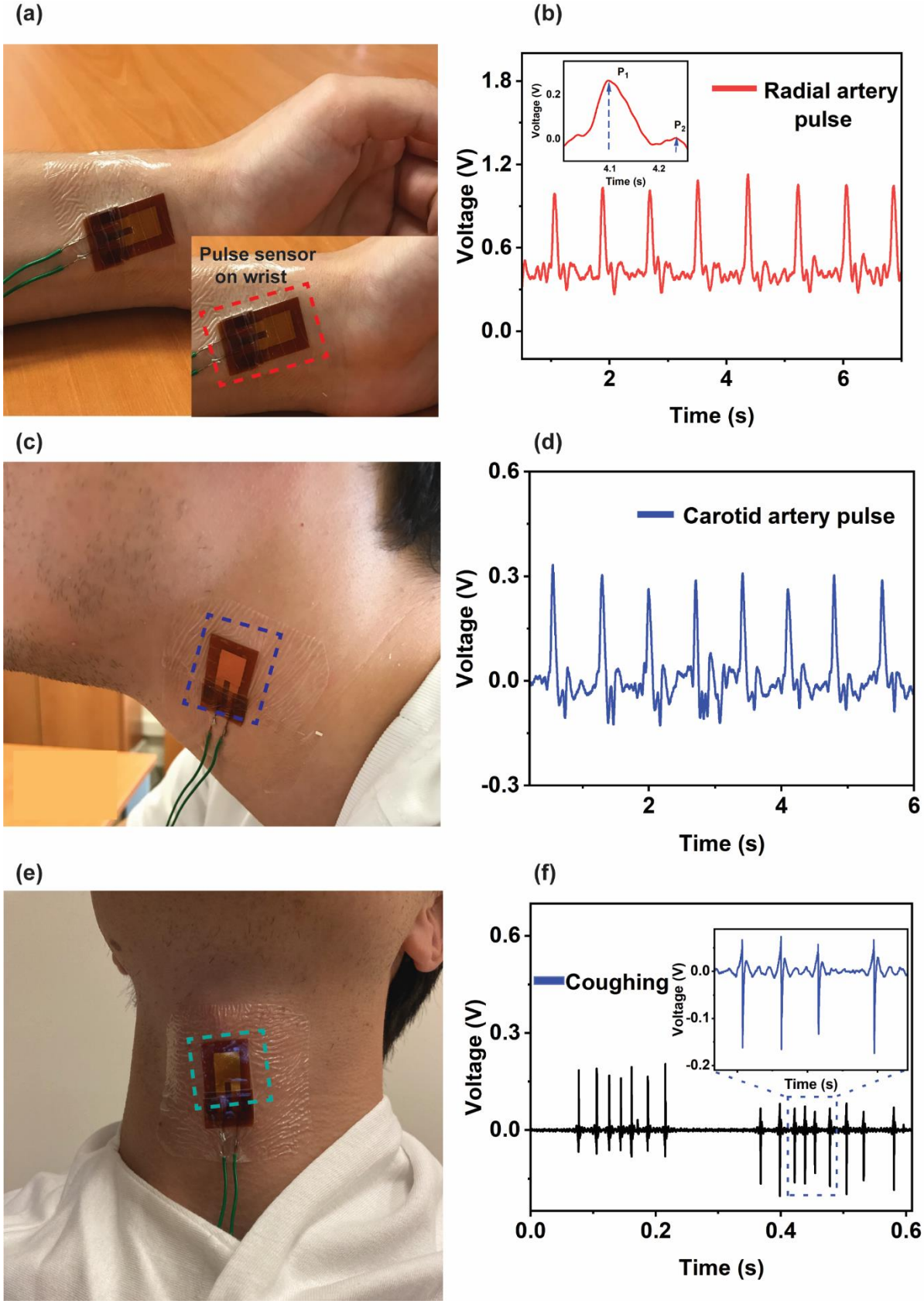

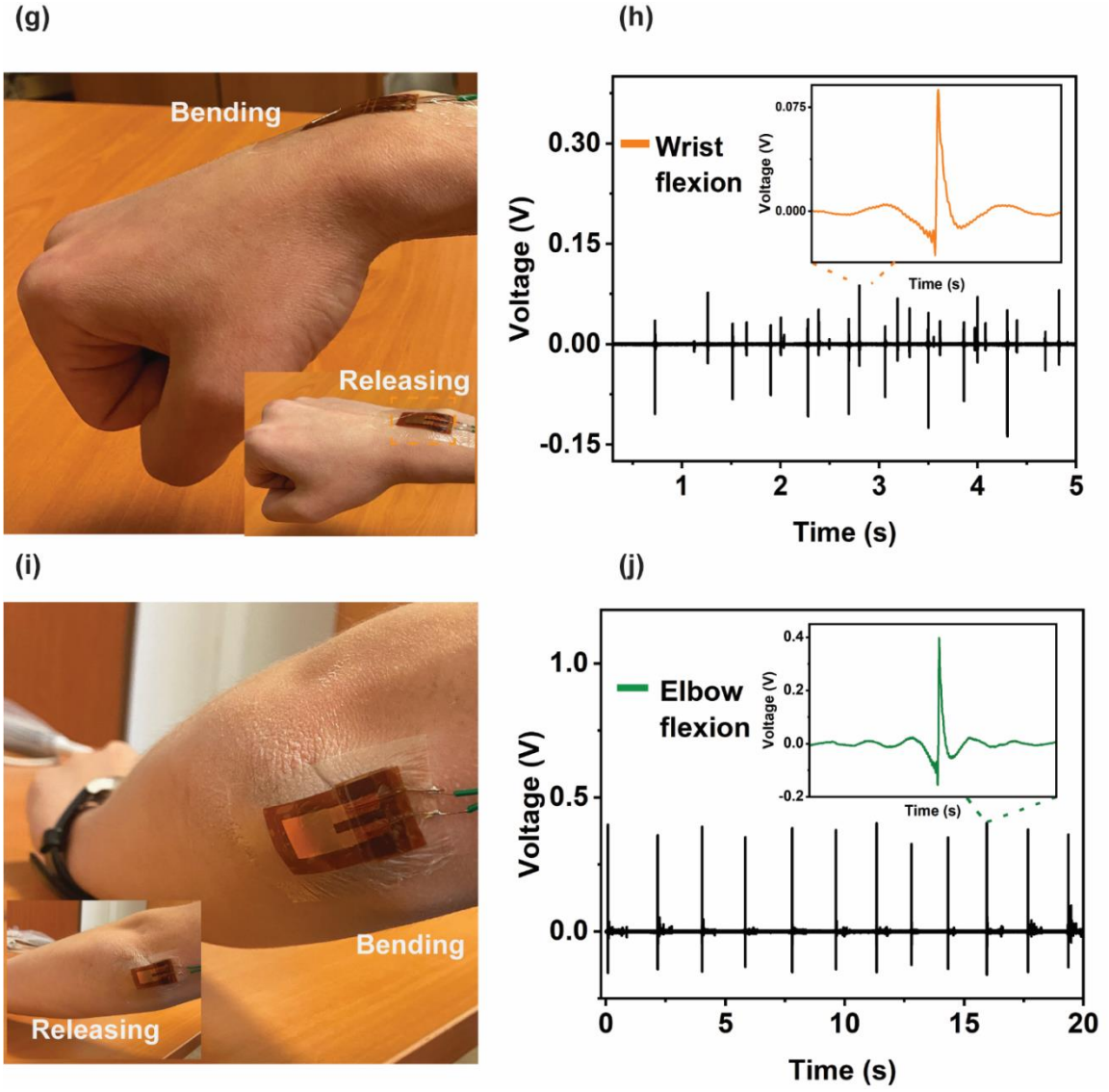

Figure 4-10*: a) Image of piezoelectric sensor conformally affixed to human wrist through a biocompatible adhesive (3M Tegaderm). The inset displays the wearable sensor consistent with the movement of the blood vessel. b) Signals detected by the PLLA/Gly-10 sensor from radial artery pulse, demonstrating different heart rates and produced voltage output under normal conditions. The inset shows enlarged voltage signals by the radial artery pulse, indicating pulse pressure (P_1) and late systolic augmentation (P_2). c) Image of piezoelectric sensor conformally affixed to the carotid artery position. d) The signals generated in response to the pressure produced by the carotid artery. e) Photograph of the piezoelectric sensor attached around the throat for monitoring strain instigated by muscle movement for the vibration of vocal cord (f) (coughing).*

Detected muscle movement in terms of voltage output. Photograph of the wearable piezoelectric sensor mounted on (g) wrist and (i) elbow joints. Detected joint motion in terms of voltage output (h) wrist and (j) elbow.

4.5 Current and power density measurement

The wearable sensor could also power bioelectronics by harvesting small-scale mechanical energies. The power density and current output of the sensor are measured as a function of different resistances (R_L) ranging from 100 KΩ to 10 MΩ (under 6Hz frequency). **Figure 4.11**a. shows, as the resistance increases, the current through the load resistance decreases from short circuit current. In contrast, when the resistance becomes infinitely large, the voltage across the load enhances and gets saturates to open circuit voltage. The following relation, $P = \frac{V^2}{A \cdot R_L}$ was used to compute the output power density. Where, V is the voltage drop across R_L, and A is the effective area of the sensor. The power density of PLLA/GLy-10 sensor as a function of varying resistance is depicted in **Figure 4.11**b. The maximum value of power density (4.17 x 10^{-5} mW/m^2) was achieved at 400 kΩ of load resistance.

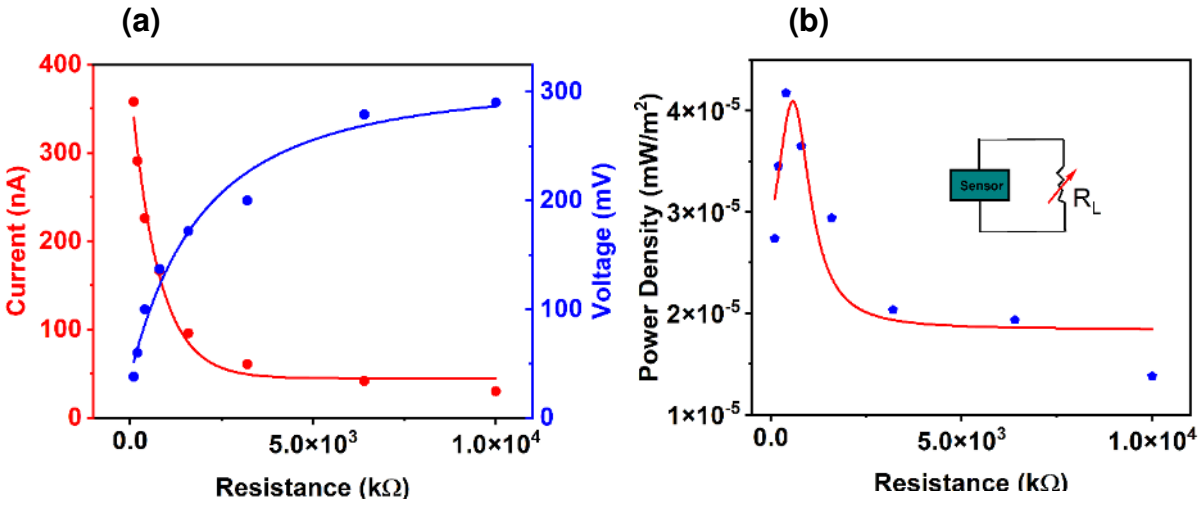

Figure 4-11*: a) Change in current, output voltage and (b) instantaneous output power density as a funciton of load resistances ranging from 100 kΩ- 10 MΩ.*

4.7 Biodegradation of PLLA/Gly-10 film

In this study, we used non-degradable materials for encapsulation and electrodes to assess the piezoelectricity of biodegradable PLLA/Gly film due to the durability, flexibility, and easy fabrication method. Owing to the biodegradable nature of both the materials (PLLA and glycine) utilized in this study, it is important to estimate the rate of degradation of the PLLA/Gly film. The bioresorption of PLLA mainly depends on the temperature and pH.[221] Chen et al.[222] reported that PLLA exhibits quite slow degradation in PBS (pH = 7.4) at room temperature, dropping only 5% of its initial weight after 6 weeks. They also demonstrated that the incorporation of other monomers into PLLA matrix significantly increased the degradation rate (lost more than 20% of initial weight). In this regard, degradation behaviour of piezoelectric PLLA/Gly film was studied by submerging it in a phosphate-buffered saline (PBS) solution at 37 ºC, as shown in **Figure 4.12**. Because of the slow bioresorption rate of PLLA in PBS with 7.4 pH, an accelerated degradation test was carried out at a pH of 12. The accelerated bioreorption test depicts the full dissolution of PLLA/Gly film in 5 days (Movie S7, SI). We investigated that the degradation rate of PLLA/Gly film in PBS (pH=12), is higher than the degradation rate of PLLA in PBS (pH=7.4).[222] It can also be stated that the bioresorption rate of PLLA/Gly film enhanced significantly due to the incorporation of glycine in PLLA matrix. This may be attributed to the hydrolysis of ester group as well as imine groups resulted in the degradation of PLLA/Gly which caused extra mass lose, while hydrolysis of the ester-bond backbone resulted in the degradation of PLLA.[223]

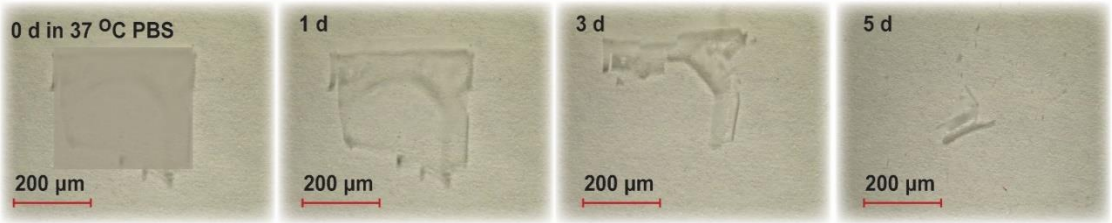

Figure 4-12**:** *Optical images showing the biodegradability of piezoelectric PLLA/Gly film in PBS solution with time. The piezoelectric film completely degraded in PBS solution at 37 °C after 5 days.*

Chapter 5:
COCLUSION

In this thesis, a systematic study for the fabrication of a wearable self-powered piezoelectric sensor based on a novel biodegradable piezoelectric material (PLLA/Gly-10) prepared by a simple and efficient method was carried out. The PLLA/Gly-10 thin film (~15 µm) obtained by a spin coating process was sandwiched between two aluminum electrodes, followed by encapsulation with Kapton tape. The sensor demonstrated a sensitivity of (~0.01322 kPa^{-1}), 10 ms response time, and good long-term stability over 4000 impact cycles. The wearable sensor also responded to vibrations generated at 41 Hz.

The sensor was conformally affixed to the human epidermis and monitored the radial/carotid artery pulse, human motion activities, and muscle movements. The acquired results suggest that PLLA/Gly-10 composite is a new promising biodegradable piezoelectric material for sensing applications. Compared with the sensor assembled with photolithography, the simple fabrication method makes the sensor more favourable. However, the fabrication method can be explored further to improve the piezoelectric properties.

Furthermore, the biodegradable nature of the film makes the sensor a good alternative environment-friendly application, especially in healthcare applications where the maintenance of hygiene conditions is critical. Because of the biodegradability of piezoelectric PLLA/Gly film, it could be utilized to fabricate fully biodegradable/implantable biomedical devices for monitoring important bio-physiological pressures inside the body, allowing the development of new types of tissues and organs. In addition, the piezoelectricity of PLLA/Gly might be useful for generating voltage from biological deformations to offer an important electrical simulation for the regeneration/repair of tissue, for example, wound healing.

Perspectives

Despite having all these intriguing potential abilities, both synthetic and nature-derived polymers are still experiencing challenges below:

(1) Long-term stability has excellent importance for bio-decomposable piezoelectric polymers. Polymorphs of most of the amino acid-based polymers having considerable piezoelectricity are metastable. For instance, transformation of β-glycine to γ and α-glycine occurs at room temperature. Moreover, several biomedical devices must pass through several strain cycles, reducing the piezoelectric performance of peptides-based polymers containing low stability. In addition, high temperature is of great concern for most biological materials as they cannot continuously exist in harsh environments. Using synthetic PLLA above 60 ºC could also be problematic as its low glass transition temperature is at ~60 ºC.[224,225] A solution to this problem could be a strong encapsulation layer that can improve stability and durability.

(2) Many of the applications of biodegradable piezoelectric polymers, including scaffolds, sensors, nanogenerators, and ultrasonic transducers, all need bulk-scale material building blocks. To develop more practical devices, it is necessary to introduce effective techniques for fabricating high-quality bioresorbable piezoelectric materials. Evolving processes, such as additive manufacturing, are anticipated to offer much ease in material preparation and device manufacturing. Utilizing machine learning advances and state-of-the-art data science, we may introduce more instructive blueprints for the preparation of materials.

Regardless of such challenges, the field of bioresorbable piezoelectric materials is expanding quickly. Considering the current development in material science and the biomedical engineering field, innovative solutions will assist in overcoming such challenges in the future to alleviate the implementation of biodegradable piezoelectric material in the biomedical engineering field. The latest improvements in the development of biodegradable piezoelectric polymers and manufacturing will continue to introduce efficient treatments in medicine and new diagnostic tools. Bioresorbable piezoelectric polymers hold great potential as an impending group of functional polymers for electromechanical applications. Their intrinsic features place them at the top position for biomedical applications with environmental sustainability, biosafety, and incomparable biocompatibility. Many exciting research opportunities based on biodegradable

piezoelectric materials will introduce groundbreaking basic understandings. We expect the natural and synthetic bio-piezoelectric polymers group will soon emerge as a potential interdisciplinary subfield at the junction between biomedical engineering and material science.

BIBLIOGRAPHY

[1] H. Cui, R. Hensleigh, D. Yao, D. Maurya, P. Kumar, M. G. Kang, S. Priya, X. R. Zheng, *Nat. Mater.* **2019**, *18*, 234.

[2] M. De Jong, W. Chen, H. Geerlings, M. Asta, K. A. Persson, *Sci. data* **2015**, *2*, 1.

[3] B. Malic, T. Rojac, *Nat. Mater.* **2018**, *17*, 297.

[4] M. T. Chorsi, E. J. Curry, H. T. Chorsi, R. Das, J. Baroody, P. K. Purohit, H. Ilies, T. D. Nguyen, *Adv. Mater.* **2019**, *31*, 1802084.

[5] K. S. Ramadan, D. Sameoto, S. Evoy, *Smart Mater. Struct.* **2014**, *23*, 33001.

[6] N. Sezer, M. Koç, *Nano Energy* **2021**, *80*, 105567.

[7] H. Yuan, T. Lei, Y. Qin, R. Yang, *Nano Energy* **2019**, *59*, 84.

[8] F. Jiang, X. Zhou, J. Lv, J. Chen, J. Chen, H. Kongcharoen, Y. Zhang, P. S. Lee, *Adv. Mater.* **2022**, *34*, 2200042.

[9] R. Singh, M. J. Bathaei, E. Istif, L. Beker, *Adv. Healthc. Mater.* **2020**, *9*, 2000790.

[10] V. L. Stuber, D. B. Deutz, J. Bennett, D. Cannel, D. M. de Leeuw, S. van der Zwaag, P. Groen, *Energy Technol.* **2019**, *7*, 177.

[11] F. Rubio-Marcos, J. F. Fernandez, D. A. Ochoa, J. E. García, R. E. Rojas-Hernandez, M. Castro, L. Ramajo, *J. Eur. Ceram. Soc.* **2017**, *37*, 3501.

[12] T. Zheng, J. Wu, D. Xiao, J. Zhu, *Prog. Mater. Sci.* **2018**, *98*, 552.

[13] R. A. Surmenev, R. V Chernozem, I. O. Pariy, M. A. Surmeneva, *Nano Energy* **2021**, *79*, 105442.

[14] F. Liu, N. A. Hashim, Y. Liu, M. R. M. Abed, K. Li, *J. Memb. Sci.* **2011**, *375*, 1.

[15] J. Lu, S. Hu, W. Li, X. Wang, X. Mo, X. Gong, H. Liu, W. Luo, W. Dong, C. Sima, Y. Wang, G. Yang, J. T. Luo, S. Jiang, Z. Shi, G. Zhang, *ACS Nano* **2022**,

16, 3744.

[16] M. Mohammadkhah, D. Marinkovic, M. Zehn, S. Checa, *Bone* **2019**, *127*, 544.

[17] A. C. Ahn, A. J. Grodzinsky, *Med. Eng. Phys.* **2009**, *31*, 733.

[18] M. Minary-Jolandan, M.-F. Yu, *Nanotechnology* **2009**, *20*, 85706.

[19] J. Sun, H. Guo, J. Ribera, C. Wu, K. Tu, M. Binelli, G. Panzarasa, F. W. M. R. Schwarze, Z. L. Wang, I. Burgert, *ACS Nano* **2020**, *14*, 14665.

[20] Z. Fang, H. Zhang, S. Qiu, Y. Kuang, J. Zhou, Y. Lan, C. Sun, G. Li, S. Gong, Z. Ma, *Adv. Mater. Technol.* **2021**, *6*, 2000928.

[21] J. Sun, H. Guo, G. N. Schädli, K. Tu, S. Schär, F. W. M. R. Schwarze, G. Panzarasa, J. Ribera, I. Burgert, *Sci. Adv.* **2021**, *7*, eabd9138.

[22] E. J. Curry, K. Ke, M. T. Chorsi, K. S. Wrobel, A. N. Miller, A. Patel, I. Kim, J. Feng, L. Yue, Q. Wu, *Proc. Natl. Acad. Sci.* **2018**, *115*, 909.

[23] G. Ico, A. Myung, B. S. Kim, N. V Myung, J. Nam, *Nanoscale* **2018**, *10*, 2894.

[24] Z. L. Wang, J. Song, *Science (80-.).* **2006**, *312*, 242.

[25] X. Song, F. Hui, K. Gilmore, B. Wang, G. Jing, Z. Fan, E. Grustan-Gutierrez, Y. Shi, L. Lombardi, S. A. Hodge, *Nanoscale* **2017**, *9*, 6237.

[26] C. Dagdeviren, Y. Shi, P. Joe, R. Ghaffari, G. Balooch, K. Usgaonkar, O. Gur, P. L. Tran, J. R. Crosby, M. Meyer, *Nat. Mater.* **2015**, *14*, 728.

[27] L. Y. Chen, B. C.-K. Tee, A. L. Chortos, G. Schwartz, V. Tse, D. J Lipomi, H.-S. P. Wong, M. V McConnell, Z. Bao, *Nat. Commun.* **2014**, *5*, 1.

[28] S. Imani, A. J. Bandodkar, A. M. Mohan, R. Kumar, S. Yu, J. Wang, P. P. Mercier, *Nat. Commun.* **2016**, *7*, 1.

[29] T. Q. Trung, S. Ramasundaram, B. Hwang, N. Lee, *Adv. Mater.* **2016**, *28*, 394.

[30] X. Wang, Y. Gu, Z. Xiong, Z. Cui, T. Zhang, *Adv. Mater.* **2014**, *26*, 1336.

[31] J. T. Muth, D. M. Vogt, R. L. Truby, Y. Mengüç, D. B. Kolesky, R. J. Wood, J. A. Lewis, *Adv. Mater.* **2014**, *26*, 6307.

[32] J.-W. Seo, M. Joo, J. Ahn, T.-I. Lee, T.-S. Kim, S. G. Im, J.-Y. Lee, *Nanoscale* **2017**, *9*, 3399.

[33] Y. Wang, L. Wang, T. Yang, X. Li, X. Zang, M. Zhu, K. Wang, D. Wu, H. Zhu, *Adv. Funct. Mater.* **2014**, *24*, 4666.

[34] M. Ma, Z. Zhang, Q. Liao, F. Yi, L. Han, G. Zhang, S. Liu, X. Liao, Y. Zhang, *Nano Energy* **2017**, *32*, 389.

[35] H. He, H. Zeng, Y. Fu, W. Han, Y. Dai, L. Xing, Y. Zhang, X. Xue, *J. Mater. Chem. C* **2018**, *6*, 9624.

[36] Y. Dai, Y. Fu, H. Zeng, L. Xing, Y. Zhang, Y. Zhan, X. Xue, A. S.-P. B.-L. Vision, *Adv. Funct. Mater* **2018**, *28*, 1800275.

[37] G. Schwartz, B. C.-K. Tee, J. Mei, A. L. Appleton, D. H. Kim, H. Wang, Z. Bao, *Nat. Commun.* **2013**, *4*, 1.

[38] C. M. Boutry, A. Nguyen, Q. O. Lawal, A. Chortos, S. Rondeau-Gagné, Z. Bao, *Adv. Mater.* **2015**, *27*, 6954.

[39] S. C. B. Mannsfeld, B. C. K. Tee, R. M. Stoltenberg, C. V Chen, S. Barman, B. V. O. Muir, A. N. Sokolov, C. Reese, Z. Bao, *Nat. Mater.* **2010**, *9*, 859.

[40] L. Pan, A. Chortos, G. Yu, Y. Wang, S. Isaacson, R. Allen, Y. Shi, R. Dauskardt, Z. Bao, *Nat. Commun.* **2014**, *5*, 1.

[41] C. Choong, M. Shim, B. Lee, S. Jeon, D. Ko, T. Kang, J. Bae, S. H. Lee, K. Byun, J. Im, *Adv. Mater.* **2014**, *26*, 3451.

[42] W. Gao, S. Emaminejad, H. Y. Y. Nyein, S. Challa, K. Chen, A. Peck, H. M. Fahad, H. Ota, H. Shiraki, D. Kiriya, *Nature* **2016**, *529*, 509.

[43] S. Gong, W. Schwalb, Y. Wang, Y. Chen, Y. Tang, J. Si, B. Shirinzadeh, W. Cheng, *Nat. Commun.* **2014**, *5*, 1.

[44] Y. Ma, Q. Zheng, Y. Liu, B. Shi, X. Xue, W. Ji, Z. Liu, Y. Jin, Y. Zou, Z. An, *Nano Lett.* **2016**, *16*, 6042.

[45] Y. Mao, P. Zhao, G. McConohy, H. Yang, Y. Tong, X. Wang, *Adv. Energy Mater.* **2014**, *4*, 1301624.

[46] C. Pan, L. Dong, G. Zhu, S. Niu, R. Yu, Q. Yang, Y. Liu, Z. L. Wang, *Nat. Photonics* **2013**, *7*, 752.

[47] X. Wang, H. Zhang, L. Dong, X. Han, W. Du, J. Zhai, C. Pan, Z. L. Wang, *Adv. Mater.* **2016**, *28*, 2896.

[48] X. Wang, M. Que, M. Chen, X. Han, X. Li, C. Pan, Z. L. Wang, *Adv. Mater.* **2017**, *29*, 1605817.

[49] S. Jung, J. Lee, T. Hyeon, M. Lee, D. Kim, *Adv. Mater.* **2014**, *26*, 6329.

[50] S. H. Lee, C. K. Jeong, G.-T. Hwang, K. J. Lee, *Nano Energy* **2015**, *14*, 111.

[51] F. Yi, Z. Zhang, Z. Kang, Q. Liao, Y. Zhang, *Adv. Funct. Mater.* **2019**, *29*, 1808849.

[52] C. Lee, T. Itoh, T. Suga, *IEEE Trans. Ultrason. Ferroelectr. Freq. Control* **1996**, *43*, 553.

[53] C. W. Chee, C.-H. Wong, Z. Dahari, in *2016 IEEE Reg. 10 Conf.*, IEEE, **2016**, pp. 3771–3774.

[54] Y. Fu, H. He, T. Zhao, Y. Dai, W. Han, J. Ma, L. Xing, Y. Zhang, X. Xue, *Nano-micro Lett.* **2018**, *10*, 1.

[55] S. Gong, B. Zhang, J. Zhang, Z. L. Wang, K. Ren, *Adv. Funct. Mater.* **2020**, *30*, 1908724.

[56] Y. Saito, H. Takao, T. Tani, T. Nonoyama, K. Takatori, T. Homma, T. Nagaya, M. Nakamura, *Nature* **2004**, *432*, 84.

[57] N. Mehmood, A. Hariz, S. Templeton, N. H. Voelcker, *Sensors* **2014**, *14*, 21770.

[58] E. S. Hosseini, L. Manjakkal, R. Dahiya, in *2018 IEEE SENSORS*, IEEE, **2018**, pp. 1–4.

[59] C. García Núñez, L. Manjakkal, R. Dahiya, *npj Flex. Electron.* **2019**, *3*, 1.

[60] V. Nguyen, R. Zhu, K. Jenkins, R. Yang, *Nat. Commun.* **2016**, *7*, 1.

[61] M. Minary-Jolandan, M.-F. Yu, *Biomacromolecules* **2009**, *10*, 2565.

[62] A. Heredia, V. Meunier, I. K. Bdikin, J. Gracio, N. Balke, S. Jesse, A. Tselev, P. K. Agarwal, B. G. Sumpter, S. V Kalinin, *Adv. Funct. Mater.* **2012**, *22*, 2996.

[63] B. Y. Lee, J. Zhang, C. Zueger, W.-J. Chung, S. Y. Yoo, E. Wang, J. Meyer, R. Ramesh, S.-W. Lee, *Nat. Nanotechnol.* **2012**, *7*, 351.

[64] M. Smith, Y. Calahorra, Q. Jing, S. Kar-Narayan, *APL Mater.* **2017**, *5*, 74105.

[65] E. Fukada, *Jpn. J. Appl. Phys.* **1998**, *37*, 2775.

[66] M. Ando, H. Kawamura, K. Kageyama, Y. Tajitsu, *Jpn. J. Appl. Phys.* **2012**, *51*, 09LD14.

[67] Y. Tajitsu, S. Kawai, M. Kanesaki, M. Date, E. Fukada, *Ferroelectrics* **2004**, *304*, 195.

[68] E. Fukada, *Biorheology* **1995**, *32*, 593.

[69] J. Kobayashi, T. Asahi, M. Ichiki, A. Oikawa, H. Suzuki, T. Watanabe, E. Fukada, Y. Shikinami, *J. Appl. Phys.* **1995**, *77*, 2957.

[70] Y. Ikada, Y. Shikinami, Y. Hara, M. Tagawa, E. Fukada, *J. Biomed. Mater. Res. An Off. J. Soc. Biomater. Japanese Soc. Biomater.* **1996**, *30*, 553.

[71] M. Yoshida, T. Onogi, K. Onishi, T. Inagaki, Y. Tajitsu, *Jpn. J. Appl. Phys.* **2014**, *53*, 09PC02.

[72] Y. Inuzuka, K. Onishi, S. Kinoshita, Y. Nakashima, T. Nagata, H. Yamane, T. Nakai, T. Kataoka, S. Ito, Y. Tajitsu, *Jpn. J. Appl. Phys.* **2012**, *51*, 09LD15.

[73] J. Zhang, S. Gong, C. Wang, D. Jeong, Z. L. Wang, K. Ren, *Macromol. Mater. Eng.* **2019**, *304*, 1900259.

[74] Y. Tajitsu, *Ferroelectrics* **2016**, *499*, 36.

[75] E. Fukada, *IEEE Trans. Ultrason. Ferroelectr. Freq. Control* **2000**, *47*, 1277.

[76] Q. Y. Pan, S. T. S. Tasaka, N. I. N. Inagaki, *Jpn. J. Appl. Phys.* **1996**, *35*, L1442.

[77] M. Ando, H. Kawamura, H. Kitada, Y. Sekimoto, T. Inoue, Y. Tajitsu, *Jpn. J. Appl. Phys.* **2013**, *52*, 09KD17.

[78] M. Ando, H. Kawamura, H. Kitada, Y. Sekimoto, T. Inoue, Y. Tajitsu, in *2013 Jt. IEEE Int. Symp. Appl. Ferroelectr. Work. Piezoresponse Force Microsc.*, IEEE, **2013**, pp. 236–239.

[79] K. S. Anderson, M. A. Hillmyer, *Polymer (Guildf).* **2006**, *47*, 2030.

[80] S. C. Schmidt, M. A. Hillmyer, *J. Polym. Sci. Part B Polym. Phys.* **2001**, *39*, 300.

[81] H. Yamane, K. Sasai, *Polymer (Guildf).* **2003**, *44*, 2569.

[82] H. Tsuji, H. Takai, N. Fukuda, H. Takikawa, *Macromol. Mater. Eng.* **2006**, *291*, 325.

[83] H. Tsuji, H. Takai, S. K. Saha, *Polymer (Guildf).* **2006**, *47*, 3826.

[84] N. Rahman, T. Kawai, G. Matsuba, K. Nishida, T. Kanaya, H. Watanabe, H. Okamoto, M. Kato, A. Usuki, M. Matsuda, *Macromolecules* **2009**, *42*, 4739.

[85] J. Narita, M. Katagiri, H. Tsuji, *Macromol. Mater. Eng.* **2011**, *296*, 887.

[86] C. M. Boutry, L. Beker, Y. Kaizawa, C. Vassos, H. Tran, A. C. Hinckley, R. Pfattner, S. Niu, J. Li, J. Claverie, *Nat. Biomed. Eng.* **2019**, *3*, 47.

[87] J.-K. Chang, H.-P. Chang, Q. Guo, J. Koo, C.-I. Wu, J. A. Rogers, *Adv. Mater.* **2018**, *30*, 1704955.

[88] S. K. Ghosh, D. Mandal, *Nano Energy* **2016**, *28*, 356.

[89] S. K. Ghosh, D. Mandal, *Appl. Phys. Lett.* **2017**, *110*, 123701.

[90] E. Fukada, I. Yasuda, *J. Phys. Soc. Japan* **1957**, *12*, 1158.

[91] E. Fukada, S. Sasaki, *J. Polym. Sci. Polym. Phys. Ed.* **1975**, *13*, 1845.

[92] Z. Zhao, Y. Dai, S. X. Dou, J. Liang, *Mater. Today Energy* **2021**, *20*, 100690.

[93] D. Vasilescu, R. Cornillon, G. Mallet, *Nature* **1970**, *225*, 635.

[94] V. V Lemanov, *Ferroelectrics* **2000**, *238*, 211.

[95] V. V Lemanov, S. N. Popov, *Phys. Solid State* **1998**, *40*, 991.

[96] V. V Lemanov, S. N. Popov, G. A. Pankova, *Phys. Solid State* **2002**, *44*, 1929.

[97] V. V Lemanov, S. N. Popov, G. A. Pankova, *Phys. Solid State* **2011**, *53*, 1191.

[98] F. Okosun, S. Guerin, M. Celikin, V. Pakrashi, *Cell Reports Phys. Sci.* **2021**, *2*, 100434.

[99] E. S. Hosseini, L. Manjakkal, D. Shakthivel, R. Dahiya, *ACS Appl. Mater. Interfaces* **2020**, *12*, 9008.

[100] A. G. Kordlar, J. Koohsorkhi, E. T. Nejad, *Solid. State. Electron.* **2021**, *186*, 108168.

[101] L. Qiao, G. Li, H. Tao, J. Wu, Z. Xu, F. Li, *Ceram. Int.* **2020**, *46*, 5641.

[102] A. B. M. Buanz, S. Gaisford, *Cryst. Growth Des.* **2017**, *17*, 1245.

[103] A. V Gerasimov, L. S. Zubaidullina, A. S. Safiullina, R. N. Nagrimanov, M. A. Ziganshin, A. E. Boldyrev, in *AIP Conf. Proc.*, AIP Publishing LLC, **2022**, p. 30020.

[104] M. E. Lines, A. M. Glass, *Principles and Applications of Ferroelectrics and Related Materials*, Oxford University Press, **2001**.

[105] J. Li, Y. Liu, Y. Zhang, H.-L. Cai, R.-G. Xiong, *Phys. Chem. Chem. Phys.* **2013**,

15, 20786.

[106] V. S. Bystrov, E. Seyedhosseini, S. Kopyl, I. K. Bdikin, A. L. Kholkin, *J. Appl. Phys.* **2014**, *116*, 66803.

[107] S. Horiuchi, Y. Tokunaga, G. Giovannetti, S. Picozzi, H. Itoh, R. Shimano, R. Kumai, Y. Tokura, *Nature* **2010**, *463*, 789.

[108] V. S. Bystrov, E. Seyedhosseini, I. Bdikin, S. Kopyl, S. M. Neumayer, J. Coutinho, A. L. Kholkin, *Ferroelectrics* **2015**, *475*, 107.

[109] D. Vasileva, S. Vasilev, A. L. Kholkin, V. Y. Shur, *Materials (Basel).* **2019**, *12*, 1223.

[110] E. Fischer, E. Fischer, E. Fourneau, *Ueber Einige Derivate Des Glykocolls*, Springer, **1906**.

[111] S. Guerin, J. O'Donnell, E. U. Haq, C. McKeown, C. Silien, F. M. F. Rhen, T. Soulimane, S. A. M. Tofail, D. Thompson, *Phys. Rev. Lett.* **2019**, *122*, 47701.

[112] S. Vasilev, P. Zelenovskiy, D. Vasileva, A. Nuraeva, V. Y. Shur, A. L. Kholkin, *J. Phys. Chem. Solids* **2016**, *93*, 68.

[113] K. Jenkins, S. Kelly, V. Nguyen, Y. Wu, R. Yang, *Nano Energy* **2018**, *51*, 317.

[114] K. Ryan, J. Beirne, G. Redmond, J. I. Kilpatrick, J. Guyonnet, N.-V. Buchete, A. L. Kholkin, B. J. Rodriguez, *ACS Appl. Mater. Interfaces* **2015**, *7*, 12702.

[115] A. Kholkin, N. Amdursky, I. Bdikin, E. Gazit, G. Rosenman, *ACS Nano* **2010**, *4*, 610.

[116] S. Safaryan, V. Slabov, S. Kopyl, K. Romanyuk, I. Bdikin, S. Vasilev, P. Zelenovskiy, V. Y. Shur, E. A. Uslamin, E. A. Pidko, *ACS Appl. Mater. Interfaces* **2018**, *10*, 10543.

[117] V. Nguyen, K. Jenkins, R. Yang, *Nano Energy* **2015**, *17*, 323.

[118] Z. Tao, H. Yuan, S. Ding, Y. Wang, W. Hu, R. Yang, *Nano Energy* **2021**, *88*,

106229.

[119] Y. Kim, H. Park, Y. Kim, C. Lee, H. Park, J.-H. Lee, *ACS Appl. Mater. Interfaces* **2022**, *14*, 38778.

[120] H. Park, Y. Kim, Y. Kim, C. Lee, H. Park, H. Joo, J. H. Lee, J.-H. Lee, *Appl. Surf. Sci.* **2023**, *618*, 156588.

[121] I. Bdikin, V. Bystrov, *Appl. Phys. Lett* **2012**, *100*, 43702.

[122] A. Handelman, P. Beker, E. Mishina, S. Semin, N. Amdursky, G. Rosenman, *Ferroelectrics* **2012**, *430*, 84.

[123] Z. Gan, X. Wu, X. Zhu, J. Shen, *Angew. Chemie Int. Ed.* **2013**, *52*, 2055.

[124] V. S. Bystrov, E. Paramonova, I. Bdikin, S. Kopyl, A. Heredia, R. C. Pullar, A. L. Kholkin, *Ferroelectrics* **2012**, *440*, 3.

[125] H. R. Leuchtag, *Voltage-Sensitive Ion Channels: Biophysics of Molecular Excitability*, Springer, **2008**.

[126] H. R. Leuchtag, *Ferroelectrics* **2000**, *236*, 23.

[127] V. S. Bystrov, H. R. Leuchtag, *Ferroelectrics* **1994**, *155*, 19.

[128] A. Chen, C.-D. Poon, T. J. Dingemans, E. T. Samulski, *Liq. Cryst.* **1998**, *24*, 255.

[129] A. Stapleton, M. R. Noor, J. Sweeney, V. Casey, A. L. Kholkin, C. Silien, A. A. Gandhi, T. Soulimane, S. A. M. Tofail, *Appl. Phys. Lett.* **2017**, *111*, 142902.

[130] S. Guerin, S. A. M. Tofail, D. Thompson, *NPG Asia Mater.* **2019**, *11*, 10.

[131] W. Gindl, G. Emsenhuber, J. Plackner, J. Konnerth, J. Keckes, *Biomacromolecules* **2010**, *11*, 1281.

[132] K. Kemp, J. Griffiths, S. Campbell, K. Lovell, *J. Crohn's Colitis* **2013**, *7*, e386.

[133] Y. García, Y. B. Ruiz-Blanco, Y. Marrero-Ponce, C. M. Sotomayor-Torres, *Sci. Rep.* **2016**, *6*, 1.

[134] L. Csoka, I. C. Hoeger, O. J. Rojas, I. Peszlen, J. J. Pawlak, P. N. Peralta, *ACS Macro Lett.* **2012**, *1*, 867.

[135] H. Du, W. Liu, M. Zhang, C. Si, X. Zhang, B. Li, *Carbohydr. Polym.* **2019**, *209*, 130.

[136] F. Liu, M. W. Urban, *Prog. Polym. Sci.* **2010**, *35*, 3.

[137] S. Rajala, M. Vuoriluoto, O. J. Rojas, S. Franssila, S. Tuukkanen, *Proc. XXI IMEKO World Congr., Prague, Czech Repub.* **2015**.

[138] D. Zhao, Y. Zhu, W. Cheng, W. Chen, Y. Wu, H. Yu, *Adv. Mater.* **2021**, *33*, 2000619.

[139] Y. Song, Z. Shi, G.-H. Hu, C. Xiong, A. Isogai, Q. Yang, *J. Mater. Chem. A* **2021**, *9*, 1910.

[140] A. Gaur, S. Tiwari, C. Kumar, P. Maiti, **2020**.

[141] S. Maiti, S. Kumar Karan, J. Lee, A. Kumar Mishra, B. Bhusan Khatua, J. Kon Kim, *Nano Energy* **2017**, *42*, 282.

[142] C. Miao, L. Reid, W. Y. Hamad, *Appl. Mater. Today* **2021**, *24*, 101082.

[143] S. Rajala, T. Siponkoski, E. Sarlin, M. Mettanen, M. Vuoriluoto, A. Pammo, J. Juuti, O. J. Rojas, S. Franssila, S. Tuukkanen, *ACS Appl. Mater. Interfaces* **2016**, *8*, 15607.

[144] S. Horiuchi, Y. Tokura, *Nat. Mater.* **2008**, *7*, 357.

[145] A. Amran, F. B. Ahmad, M. H. M. Akmal, A. A. M. Ralib, M. I. Bin Suhaimi, *Mater. Today Commun.* **2021**, *29*, 102919.

[146] K. Kim, M. Ha, B. Choi, S. H. Joo, H. S. Kang, J. H. Park, B. Gu, C. Park, C. Park, J. Kim, *Nano Energy* **2018**, *48*, 275.

[147] N. A. Hoque, P. Thakur, P. Biswas, M. M. Saikh, S. Roy, B. Bagchi, S. Das, P. P. Ray, *J. Mater. Chem. A* **2018**, *6*, 13848.

[148] S. M. Joseph, S. Krishnamoorthy, R. Paranthaman, J. A. Moses, C. Anandharamakrishnan, *Carbohydr. Polym. Technol. Appl.* **2021**, *2*, 100036.

[149] W. Ji, H. Yuan, B. Xue, S. Guerin, H. Li, L. Zhang, Y. Liu, L. J. W. Shimon, M. Si, Y. Cao, *Angew. Chemie* **2022**, *134*, e202201234.

[150] H. K. No, S. P. Meyers, W. Prinyawiwatkul, Z. Xu, *J. Food Sci.* **2007**, *72*, DOI 10.1111/j.1750-3841.2007.00383.x.

[151] A. K. Bharimalla, S. P. Deshmukh, N. Vigneshwaran, P. G. Patil, V. Prasad, *Polym. Plast. Technol. Eng.* **2017**, *56*, 805.

[152] S. C. M. Fernandes, C. S. R. Freire, A. J. D. Silvestre, C. Pascoal Neto, A. Gandini, L. A. Berglund, L. Salmén, *Carbohydr. Polym.* **2010**, *81*, 394.

[153] M. N. V. R. Kumar, *React. Funct. Polym.* **2000**, *46*, 1.

[154] F. B. Ahmad, M. H. M. Akmal, A. Amran, M. H. Hasni, in *IOP Conf. Ser. Mater. Sci. Eng.*, IOP Publishing, **2020**, p. 12034.

[155] A. Safari, V. F. Janas, *Ferroelectrics* **1997**, *196*, 187.

[156] A. Hänninen, S. Rajala, T. Salpavaara, M. Kellomäki, S. Tuukkanen, *Procedia Eng.* **2016**, *168*, 1176.

[157] E. Praveen, S. Murugan, K. Jayakumar, *RSC Adv.* **2017**, *7*, 35490.

[158] C. Ma, H. Wang, Y. Chi, Y. Wang, L. Jiang, N. Xu, Q. Wu, Q. Feng, X. Sun, *Appl. Mater. Today* **2021**, *22*, 100902.

[159] D. Kim, S. A. Han, J. H. Kim, J. Lee, S. Kim, S. Lee, *Adv. Mater.* **2020**, *32*, 1906989.

[160] N. More, G. Kapusetti, *Med. Hypotheses* **2017**, *108*, 10.

[161] K. Kapat, Q. T. H. Shubhra, M. Zhou, S. Leeuwenburgh, *Adv. Funct. Mater.* **2020**, *30*, 1909045.

[162] I. Chae, C. K. Jeong, Z. Ounaies, S. H. Kim, *ACS Appl. Bio Mater.* **2018**, *1*, 936.

[163] S. K. Ghosh, D. Mandal, *ACS Sustain. Chem. Eng.* **2017**, *5*, 8836.

[164] V. Vivekananthan, N. R. Alluri, Y. Purusothaman, A. Chandrasekhar, S. Selvarajan, S. J. Kim, *ACS Appl. Mater. Interfaces* **2018**, *10*, 18650.

[165] D. Denning, J. I. Kilpatrick, E. Fukada, N. Zhang, S. Habelitz, A. Fertala, M. D. Gilchrist, Y. Zhang, S. A. M. Tofail, B. J. Rodriguez, *ACS Biomater. Sci. Eng.* **2017**, *3*, 929.

[166] Z. Zhou, D. Qian, M. Minary-Jolandan, *ACS Biomater. Sci. Eng.* **2016**, *2*, 929.

[167] M. Nair, Y. Calahorra, S. Kar-Narayan, S. M. Best, R. E. Cameron, *Nanoscale* **2019**, *11*, 15120.

[168] S. Bera, S. Guerin, H. Yuan, J. O'Donnell, N. P. Reynolds, O. Maraba, W. Ji, L. J. W. Shimon, P.-A. Cazade, S. A. M. Tofail, *Nat. Commun.* **2021**, *12*, 1.

[169] D.-L. Wen, D.-H. Sun, P. Huang, W. Huang, M. Su, Y. Wang, M.-D. Han, B. Kim, J. Brugger, H.-X. Zhang, *Microsystems Nanoeng.* **2021**, *7*, 1.

[170] L. Pan, F. Wang, Y. Cheng, W. R. Leow, Y.-W. Zhang, M. Wang, P. Cai, B. Ji, D. Li, X. Chen, *Nat. Commun.* **2020**, *11*, 1.

[171] T. Yucel, P. Cebe, D. L. Kaplan, *Adv. Funct. Mater.* **2011**, *21*, 779.

[172] I. Chiesa, C. De Maria, M. R. Ceccarini, L. Mussolin, R. Coletta, A. Morabito, R. Tonin, M. Calamai, A. Morrone, T. Beccari, *ACS Appl. Mater. Interfaces* **2022**.

[173] C.-T. Pan, C.-K. Yen, M.-C. Hsieh, S.-Y. Wang, C.-H. Chien, J. C.-C. Huang, L. Lin, Y.-L. Shiue, S.-W. Kuo, *ACS Appl. Energy Mater.* **2018**, *1*, 5627.

[174] V. Sencadas, C. Garvey, S. Mudie, J. J. K. Kirkensgaard, G. Gouadec, S. Hauser, *Nano Energy* **2019**, *66*, 104106.

[175] I. W. Park, K. W. Kim, Y. Hong, H. J. Yoon, Y. Lee, D. Gwak, K. Heo, *Nanomaterials* **2020**, *10*, 93.

[176] K. Heo, H.-E. Jin, H. Kim, J. H. Lee, E. Wang, S.-W. Lee, *Nano energy* **2019**,

56, 716.

[177] D.-M. Shin, H. J. Han, W.-G. Kim, E. Kim, C. Kim, S. W. Hong, H. K. Kim, J.-W. Oh, Y.-H. Hwang, *Energy Environ. Sci.* **2015**, *8*, 3198.

[178] S. J. Lee, A. P. Arun, K. J. Kim, *Mater. Lett.* **2015**, *148*, 58.

[179] A. Farahani, A. Zarei-Hanzaki, H. R. Abedi, L. Tayebi, E. Mostafavi, *J. Funct. Biomater.* **2021**, *12*, 71.

[180] K. Asaka, H. Okuzaki, *Tokyo: Springer* **2014**, *10*, 974.

[181] G. Zhao, B. Huang, J. Zhang, A. Wang, K. Ren, Z. L. Wang, *Macromol. Mater. Eng.* **2017**, *302*, 1600476.

[182] N. B. Gakkai, Ō. B. Gakkai, **1982**.

[183] A. Farahani, A. Zarei-Hanzaki, H. R. Abedi, I. Haririan, M. Akrami, Z. Aalipour, L. Tayebi, *J. Mater. Res. Technol.* **2021**, *15*, 6356.

[184] J. Zhu, L. Jia, R. Huang, *J. Mater. Sci. Mater. Electron.* **2017**, *28*, 12080.

[185] E. J. Curry, T. T. Le, R. Das, K. Ke, E. M. Santorella, D. Paul, M. T. Chorsi, K. T. M. Tran, J. Baroody, E. R. Borges, *Proc. Natl. Acad. Sci.* **2020**, *117*, 214.

[186] P. Wu, P. Chen, C. Xu, Q. Wang, F. Zhang, K. Yang, W. Jiang, J. Feng, Z. Luo, *Nano Energy* **2022**, *102*, 107707.

[187] Y. M. Yousry, V. Wong, R. Ji, Y. Chen, S. Chen, X. Zhang, D. B. K. Lim, L. Shen, K. Yao, *Adv. Funct. Mater.* **2023**, 2213582.

[188] T. T. Le, E. J. Curry, T. Vinikoor, R. Das, Y. Liu, D. Sheets, K. T. M. Tran, C. J. Hawxhurst, J. F. Stevens, J. N. Hancock, *Adv. Funct. Mater.* **2022**, 2113040.

[189] F. Yang, J. Li, Y. Long, Z. Zhang, L. Wang, J. Sui, Y. Dong, Y. Wang, R. Taylor, D. Ni, *Science (80-.).* **2021**, *373*, 337.

[190] N. Vale, A. Ferreira, J. Matos, P. Fresco, M. J. Gouveia, *Molecules* **2018**, *23*, 2318.

[191] M. J. Carbone, M. Vanhalle, B. Goderis, P. Van Puyvelde, *J. Polym. Eng.* **2015**, *35*, 169.

[192] A. Sultana, S. K. Ghosh, V. Sencadas, T. Zheng, M. J. Higgins, T. R. Middya, D. Mandal, *J. Mater. Chem. B* **2017**, *5*, 7352.

[193] J.-F. Ru, S.-G. Yang, D. Zhou, H.-M. Yin, J. Lei, Z.-M. Li, *Macromolecules* **2016**, *49*, 3826.

[194] M. Eguchi, M. S. Angelone, H. P. Yennawar, T. E. Mallouk, *J. Phys. Chem. C* **2008**, *112*, 11280.

[195] S. K. Karan, S. Maiti, A. K. Agrawal, A. K. Das, A. Maitra, S. Paria, A. Bera, R. Bera, L. Halder, A. K. Mishra, *Nano Energy* **2019**, *59*, 169.

[196] N. K. Singh, S. K. Singh, D. Dash, P. Gonugunta, M. Misra, P. Maiti, *J. Phys. Chem. C* **2013**, *117*, 10163.

[197] C. Ribeiro, V. Sencadas, C. M. Costa, J. L. G. Ribelles, S. Lanceros-Méndez, *Sci. Technol. Adv. Mater.* **2011**.

[198] M. Smith, S. Kar-Narayan, *Int. Mater. Rev.* **2022**, *67*, 65.

[199] G. Liu, X. Zhang, D. Wang, *Adv. Mater.* **2014**, *26*, 6905.

[200] S. Saeidlou, M. A. Huneault, H. Li, C. B. Park, *Prog. Polym. Sci.* **2012**, *37*, 1657.

[201] L. Gránásy, T. Pusztai, G. Tegze, J. A. Warren, J. F. Douglas, *Phys. Rev. E* **2005**, *72*, 11605.

[202] D. A. Saravanos, P. R. Heyliger, D. A. Hopkins, *Int. J. Solids Struct.* **1997**, *34*, 359.

[203] Q. Guo, G. Z. Cao, I. Y. Shen, *J. Vib. Acoust.* **2013**, *135*.

[204] S. A. Bello, S. Malavade, C. L. Passaglia, *Ann. Biomed. Eng.* **2017**, *45*, 990.

[205] R. Fu, L. Tu, Y. Zhou, L. Fan, F. Zhang, Z. Wang, J. Xing, D. Chen, C. Deng, G. Tan, *Chem. Mater.* **2019**, *31*, 9850.

[206] C. R. Piedrahita, P. Yue, J. Cao, H. Lee, C. P. Rajapaksha, C. Feng, A. Jakli, T. Kyu, *ACS Appl. Mater. Interfaces* **2020**, *12*, 16978.

[207] Y. Yue, N. Liu, W. Liu, M. Li, Y. Ma, C. Luo, S. Wang, J. Rao, X. Hu, J. Su, *Nano Energy* **2018**, *50*, 79.

[208] Z. Chen, Z. Wang, X. Li, Y. Lin, N. Luo, M. Long, N. Zhao, J.-B. Xu, *ACS Nano* **2017**, *11*, 4507.

[209] L.-Q. Tao, K.-N. Zhang, H. Tian, Y. Liu, D.-Y. Wang, Y.-Q. Chen, Y. Yang, T.-L. Ren, *ACS Nano* **2017**, *11*, 8790.

[210] C. Ma, D. Xu, Y.-C. Huang, P. Wang, J. Huang, J. Zhou, W. Liu, S.-T. Li, Y. Huang, X. Duan, *ACS Nano* **2020**, *14*, 12866.

[211] C. Ning, K. Dong, R. Cheng, J. Yi, C. Ye, X. Peng, F. Sheng, Y. Jiang, Z. L. Wang, *Adv. Funct. Mater.* **2021**, *31*, 2006679.

[212] M. Zhu, Q. Shi, T. He, Z. Yi, Y. Ma, B. Yang, T. Chen, C. Lee, *ACS Nano* **2019**, *13*, 1940.

[213] W. Deng, T. Yang, L. Jin, C. Yan, H. Huang, X. Chu, Z. Wang, D. Xiong, G. Tian, Y. Gao, *Nano Energy* **2019**, *55*, 516.

[214] S. Anwar, M. Hassanpour Amiri, S. Jiang, M. M. Abolhasani, P. R. F. Rocha, K. Asadi, *Adv. Funct. Mater.* **2021**, *31*, 2004326.

[215] M. Xu, H. Kang, L. Guan, H. Li, M. Zhang, *ACS Appl. Mater. Interfaces* **2017**, *9*, 34687.

[216] D. B. Deutz, N. T. Mascarenhas, J. B. J. Schelen, D. M. de Leeuw, S. van der Zwaag, P. Groen, *Adv. Funct. Mater.* **2017**, *27*, 1700728.

[217] S. Munir, B. Jiang, A. Guilcher, S. Brett, S. Redwood, M. Marber, P. Chowienczyk, *Am. J. Physiol. Circ. Physiol.* **2008**, *294*, H1645.

[218] W. W. Nichols, *Am. J. Hypertens.* **2005**, *18*, 3S.

[219] P. Piirila, A. R. Sovijarvi, *Eur. Respir. J.* **1995**, *8*, 1949.

[220] P. J. Fleming, R. Gilbert, Y. Azaz, P. J. Berry, P. T. Rudd, A. Stewart, E. Hall, *Br. Med. J.* **1990**, *301*, 85.

[221] L. Xu, K. Crawford, C. B. Gorman, *Macromolecules* **2011**, *44*, 4777.

[222] S. Chen, Y. Hao, W. Cui, J. Chang, Y. Zhou, *J. Mater. Sci.* **2013**, *48*, 6567.

[223] Y. H. Kim, J. H. Park, M. Lee, Y.-H. Kim, T. G. Park, S. W. Kim, *J. Control. release* **2005**, *103*, 209.

[224] C. Nakafuku, S. Takehisa, *J. Appl. Polym. Sci.* **2004**, *93*, 2164.

[225] M. Yasuniwa, S. Tsubakihara, Y. Sugimoto, C. Nakafuku, *J. Polym. Sci. Part B Polym. Phys.* **2004**, *42*, 25.

[226] A. Wang, M. Hu, L. Zhou, X. Qiang, *Nanomater. (Basel, Switzerland)* **2018**, *8*, DOI 10.3390/nano8121021.

[227] N. Chamankar, R. Khajavi, A. A. Yousefi, A. Rashidi, F. Golestanifard, *Ceram. Int.* **2020**, *46*, 19669.

[228] D. H. Kim, B. Dudem, J. S. Yu, *ACS Sustain. Chem. Eng.* **2018**, *6*, 8525.